

**Computational Fluid Dynamics (CFD) Analysis of the Burnelli CBY-3 Loadmaster**

A Major Qualifying Project Report

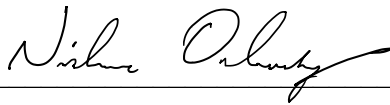
Submitted to the Faculty of the

WORCESTER POLYTECHNIC INSTITUTE

In Partial Fulfillment of the Requirements for the

Degree of Bachelor of Science

in Aerospace Engineering



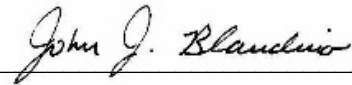
Nicholas Orlovsky

By



Maria Wojciechowski

Approved by:



John J. Blandino, Advisor  
Professor, Aerospace Engineering Department  
Worcester Polytechnic Institute

*This report represents the work of one or more WPI undergraduate students submitted to the faculty as evidence of completion of a degree requirement. WPI routinely publishes these reports on the web without editorial or peer review.*

## Abstract

This work presents a study to evaluate the lift and drag characteristics of the 1940s-era Burnelli CBY-3 Loadmaster and compare it to that of a contemporary aircraft, the Douglas DC-3. Specifically, we investigated the question of whether the Loadmaster produced more lift than the DC-3 at comparable flight conditions and second, what fraction of the Loadmaster lift was produced by the lifting-body style fuselage. The fact that no digital model of the Loadmaster airframe exists posed a unique challenge as one had to be created to perform the CFD analysis. An original methodology was developed from which archival 2D plans were photographed and imported into SolidWorks. These 2D digital sketches were then used to create the 3D geometry for the solid model. Key dimensions were checked throughout the process using both 2D drawings and the actual aircraft with the model adjusted accordingly. The solid model was imported into Ansys Fluent where the flight characteristics were evaluated at cruise velocity over a range of angles of attack. These results are summarized, and we show that the DC-3 produced more lift than the CBY-3 Loadmaster despite the extra lift provided by the unique fuselage. We believe this was in part a result of the fact that the CBY-3 design had not been fully optimized at the time the prototype was built, whereas the DC-3 was already a very mature design by the mid-1940s. Finally, we found that the lifting-body fuselage contributed approximately 30% of the total aircraft lift.

*“Certain materials are included under the fair use exemption of the U.S. Copyright Law and have been prepared according to the fair use guidelines and are restricted from further use.”*

## Acknowledgements

The MQP team would like to extend thanks to the many individuals who helped make this project possible.

- ❖ Dr. Erica S. Stults and Dr. Adriana Hera at WPI, for providing excellent and timely support with SolidWorks and Ansys Fluent.
- ❖ Professor David J. Olinger and graduate student Andrei Koch, for providing support and helpful advice.
- ❖ The staff at the New England Air Museum (NEAM), for providing us with access to the aircraft and historical records, and for making this project possible in the first place. We would especially like to express our thanks to Bob Vozzola, the NEAM Restoration Coordinator, Lou Palshaw, who helped us locate and retrieve archival documents, and two members of the Loadmaster restoration team: Doug Davis and Wayne Dow, for their invaluable insight and extensive help during our visits.
- ❖ Professor Nikolaos A. Gatsonis, Sarah Miles, and everyone at the WPI Registrar's Office, for their help in making the submission of the project on a shortened timeline possible.
- ❖ The many independent editors who offered to help us finish the project in our unexpectedly changing timeline.
  - Park Ranger Peter Orlovsky
  - Siusan Orlovsky
  - Dr. Wojciech Wojciechowski
- ❖ Members of the second Loadmaster MQP team, with whom we worked in parallel, for sharing their knowledge and experience.
  - Aaron Boyer
  - Amaya Massari
  - Jacob Moore
  - Nicholas Paszczuk
  - Emily Raynowska
  - Gabrielle Tims
- ❖ Most of all, our project advisor Professor John J. Blandino. Without his wisdom and guidance, we would have never been able to accomplish what we did.

# Table of Contents

Abstract .....	i
Acknowledgements .....	ii
List of Figures .....	v
List of Tables .....	vii
Table of Authorship .....	viii
1 Introduction .....	1
1.1 Project Goals and Objectives .....	1
1.2 Project Analysis Tasks .....	3
2 Background and Literature Review .....	4
2.1 Project Background .....	4
2.2 Introduction to CBY-3 Loadmaster and DC-3 .....	5
2.3 Aircraft Performance Metrics .....	7
2.3.1 Aircraft Historical Data Comparison .....	7
2.3.2 Aircraft Performance Calculations .....	7
3 Analysis Tools and Methods .....	14
3.1 SolidWorks .....	14
3.2 Excel Calculator for Aircraft Performance Parameters .....	14
3.3 Ansys Fluent .....	15
4 Methodology to Create a Solid Model of the CBY-3 Loadmaster .....	20
4.1 3D Laser Scanning to Create a Solid Model .....	20
4.2 Creating a Solid Model from 2D Printed Plans: Preparation .....	21
4.3 Creating a Solid Model from 2D Printed Plans: Generation of 3D Forms .....	24
4.4 Excluded Features from Model .....	28
4.5 Sourcing DC-3 Model for Comparative Analysis .....	29
5 Computational Fluid Dynamics (CFD) Analysis .....	32
5.1 Problem Description .....	32
5.1.1 Test Cases .....	32
5.1.2 Mesh Sizing .....	33
5.1.3 Enclosure Size .....	37
5.1.4 Simulation Settings and Physical Models .....	38
5.1.5 Iterations and Convergence .....	39

5.1.6	Data Collection .....	40
5.2	Results .....	42
6	Conclusions and Recommendations for Future Work .....	50
6.1	Aircraft Comparisons .....	50
6.2	Loadmaster Lifting Fuselage Properties .....	52
6.3	Recommendations for Future Work .....	52
7	References .....	55
7.1	General References .....	55
7.2	NEAM Archive Sources .....	59
8	Appendices .....	60
	Appendix A: Pictures and Description of Original Loadmaster Design Documents Used .....	60
	Appendix B: Loadmaster Key Dimensions .....	67
	Appendix C: Loadmaster Ansys Fluent Data .....	69
	Appendix D: DC-3 Ansys Fluent Data .....	69
	Appendix E: Team Gantt Chart and Organization of Tasks .....	70

## List of Figures

Figure 1: Image of CBY-3 Loadmaster [2] © NEAM, 2022 .....	5
Figure 2: Image of Douglas DC-3 [38] © David P. Henderson .....	6
Figure 3: Forces acting on an airfoil [17] © McGraw-Hill Education, 2017 .....	8
Figure 4: Representation of elliptical lift force distribution on elliptical wings. The curved dotted line represents the lift distribution. [17] © McGraw-Hill Education .....	10
Figure 5: Overview of the Pressure-Based Solution Methods [29]. © Ansys, Inc. 2009 .....	18
Figure 6: FMG Initialization [29]. ©Ansys Inc. 2009 .....	19
Figure 7: Creaform HandySCAN 3D Silver [24]. © Creaform 2022.....	20
Figure 8: Burnelli Avionics Corporation Loadmaster II [NA1] .....	22
Figure 9: Loadmaster Patent File: Front View [NA1] .....	22
Figure 10: Loadmaster Patent File: Side View [NA1].....	22
Figure 11: Loadmaster Patent File, Top View [NA1] .....	23
Figure 12: SolidWorks Layout for Loadmaster.....	24
Figure 13: Early Sketch of CBY-3 Wing in SolidWorks.....	25
Figure 14: Creation of Horizontal Stabilizer Geometry .....	26
Figure 15: Close-up View of Front of Aircraft .....	27
Figure 16: Completed Model of CBY-3 Loadmaster.....	28
Figure 17: Additional Feature found on Tail Structure of the CBY-3 .....	29
Figure 18: Original Sourced Model of the DC-3 [32] .....	30
Figure 19: Simplified DC-3 Model.....	31
Figure 20: Close-up View of Wheel Well Simplification .....	31
Figure 21: CBY-3 Surface Mesh Generation with Labeled Components .....	34
Figure 22: CBY-3 Virtual Wind Tunnel, with Bodies of Influence Visible .....	35
Figure 23: Top View of CBY-3 Virtual Wind Tunnel.....	36
Figure 24: Volume Mesh of Bodies of Influence.....	37
Figure 25: Volume Mesh Around Mid-Section of CBY-3 .....	37
Figure 26: Residual Oscillation and Non-Convergence .....	40
Figure 27: Lift Coefficient v. Angle of Attack – CBY-3 .....	42
Figure 28: Lift Coefficient v. Angle of Attack – DC-3 .....	43
Figure 29: Drag Coefficient v. Lift Coefficient (Drag Polar) – CBY-3 .....	44

Figure 30: Drag Coefficient v. Lift Coefficient (Drag Polar) - DC-3	44
Figure 31: Dynamic Pressure Distribution Around CBY-3 Centerline	46
Figure 32: Dynamic Pressure Distribution Around DC-3 Centerline	46
Figure 33: Dynamic Pressure Distribution of CBY-3 Wing, AoA = 2.5°	47
Figure 34: Dynamic Pressure Distribution of DC-3 Wing, AoA = 2.5	47
Figure 35: Pressure Coefficient Distribution on CBY-3, AoA = 2.5°	48
Figure 36: Pressure Coefficient Distribution on DC-3, Wing AoA = 2.5°	48
Figure 37: Pressure Coefficient Distribution on Bottom of CBY-3, AoA = 2.5°	49
Figure 38: Pressure Coefficient Distribution on Bottom of DC-3, Wing AoA = 2.5°	49
Figure 39: Basic Dimensions of Wing & Spars [NA2]	61
Figure 40: Descriptive View of Spar Flanges [NA3]	61
Figure 41: General Assembly: Tail Unit - Vertical Stabilizer [NA4]	62
Figure 42: General Assembly: Tail Unit: Both Stabilizers [NA4]	62
Figure 43: General Assembly: Tail Unit: Horizontal Stabilizer [NA4]	63
Figure 44: Body Layout: Stitched Together from Multiple Pictures [NA5]	64
Figure 45: Datum Points - Side View [NA6]	65
Figure 46: Datum Points - Top View [NA6]	65
Figure 47: Body Master Layout - Side and Top [NA7]	66
Figure 48: Body Master Layout – Front [NA7]	66
Figure 49: Loadmaster Dimensions - Top View	67
Figure 50: Loadmaster Dimensions - Front View	67
Figure 51: Loadmaster Dimensions - Right View	68
Figure 52: Image of the Gantt Chart used for Goal 1. Rows in the bottom of the picture correspond to the tasks in the top picture.	70
Figure 53: Image of the Gantt Chart used for Goals 2 and 3. Rows in the bottom of the picture correspond to the tasks in the top picture.	71
Figure 54: Image of the Gantt Chart used for Writing Goals. Rows in the bottom of the picture correspond to the tasks in the top picture.	72

## List of Tables

Table 1: Aircraft CAD models Analysis Task.....	3
Table 2: Aircraft CFD Analysis Task.....	3
Table 3: Aircraft Performance Characteristics from Experimental Data.....	7
Table 4: Navier-Stokes Equations Variables .....	16
Table 5: k- $\omega$ SST Equation Variables.....	17
Table 6: Loadmaster Mesh Sizing .....	34
Table 7: DC-3 Mesh Sizing .....	34
Table 8: Mesh Sizing of Simulation Volume Components .....	36
Table 9: Calculated Performance Characteristics Summary .....	45
Table 10: NEAM Archive Sources.....	59
Table 11: NEAM Archive Documents Use .....	60
Table 12: Data Collected from Ansys Fluent for Loadmaster.....	69
Table 13: Data Collected from Ansys Fluent for DC-3.....	69



## Table of Authorship

<b>Section</b>	<b>Author</b>
Abstract	Team
Acknowledgements	Team
1 Introduction	
1.1 Project Goals and Objectives	M.W
1.2 Project Analysis Tasks	M.W
2 Background and Literature Review	
2.1 Project Background	M.W
2.2 Introduction to CBY-3 Loadmaster and DC-3	M.W
2.3 Aircraft Performance Metrics	
2.3.1 Aircraft Historical Data Comparison	M.W
2.3.2 Aircraft Performance Calculations	M.W
3 Analysis Tools and Methods	
3.1 SolidWorks	Team
3.2 Excel Calculator for Aircraft Performance Parameters	M.W
3.2 Ansys Fluent	N.O
4 Methodology to Create a Solid Model of the CBY-3 Loadmaster	
4.1 3D Laser Scanning to Create a Solid Model	N.O
4.2 Creating a Solid Model from 2D Printed Plans: Preparation	N.O
4.3 Creating a Solid Model from 2D Printed Plans: Generation of 3D Forms	N.O
4.4 Excluded Features from Model	N.O
4.5 Sourcing DC-3 Model for Comparative Analysis	N.O
5 Computational Fluid Dynamics (CFD) Analysis	
5.1 Problem Description	N.O
5.1.1 Test Cases	N.O
5.1.2 Mesh Sizing	N.O
5.1.3 Enclosure Size	N.O
5.1.4 Simulation Settings and Physical Models	N.O
5.1.5 Iterations and Convergence	N.O
5.1.6 Data Collection	N.O

5.2 Results	Team
6 Conclusions and Recommendations for Future Work	
6.1 Aircraft Comparisons	Team
6.2 Loadmaster Lifting Fuselage Properties	N.O
6.3 Recommendations for Future Work	Team
7 References	
7.1 General References	Team
7.2 NEAM Archive Sources	Team
8 Appendices	Team

# 1 Introduction

## 1.1 Project Goals and Objectives

This report presents results of an investigation of the aerodynamic characteristics of the Burnelli CBY-3 Loadmaster with the intention of gaining insight into the efficacy of certain design choices. To accomplish this, three specific goals were identified:

- Evaluate how the CBY-3's aerodynamic performance would have compared to contemporary aircraft, specifically the Douglas DC-3.
- Evaluate options to convert archival print drawings and documents into an accurate 3D solid model.
- Gain insight and training in software tools that will assist in the completion of an accurate aerodynamic simulation, such as SOLIDWORKS and Ansys Fluent.

To complete the aerodynamic analysis of the CBY-3, five objectives were set and completed. These are listed below along with tasks that needed to be completed to meet the listed objective. The two most significant analytical tasks that comprised most of the effort are described in Section 1.2.

- Aircraft Research
  - Research the history of the CBY-3 Loadmaster and the Douglas DC-3
  - Research recorded performance metrics of both the CBY-3 and the DC-3
- Computational Fluid Dynamics Research
  - Review any published work describing CFD of entire aircraft and what parameters are evaluated
  - Identify how best to set up a Fluent simulation domain with appropriate boundary conditions
  - Using research, prepare a test matrix for Fluent simulations
- Computational Fluid Dynamics Analysis
  - Import both the CBY-3 and DC-3 solid models into Ansys Fluent
  - Perform Fluent simulation of both aircraft, including troubleshooting
  - Collect data from simulations to be included in results

- CAD Model Creation
  - Research and determine methodology of converting 2D blueprints into a 3D solid (CAD) model
  - Construct solid model of the CBY-3 and DC-3
- Software Training
  - Attend Ansys training sessions offered by WPI
  - Find tutorials accessible online describing how to use the software

## 1.2 Project Analysis Tasks

The overall project goals, objectives, and tasks were described in Section 1.1. Of the tasks listed, two comprise the core of the analytical work and majority of effort included in this report. The first of these was the creation of a solid model for the aircraft, required to be able to perform computational fluid dynamic analysis. The second was the problem formulation and the CFD analysis itself. These two tasks are described in Table 1 and Table 2.

Table 1: Aircraft CAD models Analysis Task

<b>Task 1: CBY-3 and DC-3 Solid Model</b>	
Problem Statement	Create a CAD solid model of the CBY-3 and import an existing model of the DC-3.
Solution Methodology	<ul style="list-style-type: none"> <li>• Tool: SOLIDWORKS</li> <li>• Use original blueprints of the CBY-3 for dimensions and geometry</li> <li>• Use a publicly accessible model of the DC-3 and edit it for aerodynamic analysis</li> </ul>
Analysis Products	<ul style="list-style-type: none"> <li>• Accurate, full-scale CAD model of CBY-3</li> <li>• Accurate, full-scale CAD model of DC-3</li> </ul>
Use of Results	<ul style="list-style-type: none"> <li>• Both models of the aircraft will be imported into Ansys Fluent for aerodynamic analysis</li> </ul>

Table 2: Aircraft CFD Analysis Task

<b>Task 2: CBY-3 and DC-3 Aerodynamic Analysis</b>	
Problem Statement	Evaluate and compare the aerodynamic efficiency <sup>1</sup> of both the CBY-3 and the DC-3 using computational fluid dynamics
Solution Methodology	<ul style="list-style-type: none"> <li>• Tool: Ansys Fluent and Microsoft Excel</li> <li>• Required Inputs: CBY-3 and DC-3 solid model, domain definition, initial and boundary conditions (angle of attack, flight velocity, altitude), fluid properties, and mesh characteristics</li> </ul>
Analysis Products	<ul style="list-style-type: none"> <li>• Lift and drag coefficients of the aircraft</li> <li>• Vertical and horizontal forces on the aircraft</li> <li>• Pressure distribution over selected surfaces</li> </ul>
Use of Results	<ul style="list-style-type: none"> <li>• Lift and coefficients and forces will be used to analyze the lift capability of each aircraft</li> <li>• Drag coefficients and forces will be used as a rough measure of efficiency of each aircraft</li> </ul>

<sup>1</sup> In this context “aerodynamic efficiency” is defined as maximizing the lift of the aircraft while minimizing the drag, enabling the plane to use less thrust and therefore less fuel to maintain cruise conditions.

## 2 Background and Literature Review

### 2.1 Project Background

Worcester Polytechnic Institute's Aerospace Engineering Department has collaborated with the New England Air Museum (NEAM) to study one of their most recent restoration projects, the CBY-3 Loadmaster. The Connecticut Aeronautical Historical Association (CAHA), parent organization of NEAM, was founded in 1960 [1]. In 1972, the museum came into possession of the CBY-3 Loadmaster, the only one ever built, and began its restoration in 2014 [2]. This aircraft has an unconventional and intriguing design which could be potentially stronger and more aerodynamically efficient than other, more common aircraft designs, like that of the Douglas DC-3. The WPI MQP team was tasked with investigating this possibility by comparing the CBY-3's and the DC-3's aerodynamic characteristics through computational fluid dynamics and analyzing the structural stresses of the wing attachment to the fuselage of both aircraft. Additionally, the team was tasked with reviewing the restoration workflow used at the NEAM as well as its use of specialized software and 3D printing techniques.

Early in the project, the WPI MQP was separated into two separate groups working on parallel and closely interrelated projects. As a part of this reorganization, one team would specifically investigate the computational fluid dynamics aspect of the project and would complete the project before the end of December. The rest of the members would concentrate on the structural analysis of the wing attachment and the review of the NEAM restoration workflow. Therefore, the sole focus of this report is the description of the aerodynamic analysis of the CBY-3 as it relates to the DC-3.

## 2.2 Introduction to CBY-3 Loadmaster and DC-3

The CBY-3 Loadmaster, shown in Figure 1, was an experimental aircraft built in 1944 by American aerospace engineer Vincent Burnelli in collaboration with the Canadian Car and Foundry [2, 6]. The cargo aircraft used an unconventional ‘lifting fuselage’ design, which means that the fuselage of the plane had an airfoil shape, enabling it to produce and contribute to the overall lift. Burnelli and his close supporter Charles Goodlin firmly believed that this design was more aerodynamically efficient due to the extra lift, and therefore, the CBY-3 could carry heavier loads than other commercial aircraft at the time [2, 3]. The large rectangular space in the fuselage could comfortably fit 24 passengers or 2,070 cubic feet of cargo weighing about 10,200 pounds [6, 5]. This boxy fuselage design was also considered to be safer than a cylindrical design because the rectangular shape was structurally stronger and the engines extending in the front of the aircraft would absorb much of the impact during a crash [6]. In addition, Goodlin, a test pilot, recalled that “It stalled beautifully. You could cut an engine, pull the stick back in your lap, and it would shudder a little and recover by itself” [3].



Figure 1: Image of CBY-3 Loadmaster [2] © NEAM, 2022

Despite this promising design, Burnelli was never able to obtain the financial backing he needed to begin production of the CBY-3, and the market for transport planes became overrun by the DC-3 as well as other more advanced planes developed for the second World War [5]. Although this could lead one to assume that the CBY-3 was created too late to be assimilated into the aviation industry, Burnelli believed his lifting fuselage was before its time, claiming that “Aviation is still in its infancy; give it a chance to grow up, and they will see that I am right. The

lifting fuselage is the first new configuration since streamlining was first introduced, and my plane carries more, carries it faster and safer” [4]. Regardless, only one CBY-3 was built, and it is currently on display at the New England Air Museum after being restored in 2014 [2].

Interestingly, the CBY-3 was built using quite unconventional methods. Nes Dobson, Chief Engineer and Program Manager of the CBY-3 program, stated that, “the CBY-3 was produced with but a fraction of the drawings and blueprints normally used in aircraft production. Instead of drawings, lines were lofted to blued steel and then the dimensions of major and even minor elements were lifted off the loft lines without having to make formal drawings” [5]. This would explain the inconsistencies between different drawings and blueprints that we noticed and that will be described further in Section 6.1. A result of this is that it made certain dimensions for the CBY-3 difficult to find, which will be explained in more detail in Section 4.

A contemporary and comparable aircraft to the CBY-3 is the Douglas DC-3, shown in Figure 2. The Douglas Aircraft Company began production of the DC-3 in 1935, almost ten years before the first and only CBY-3 prototype was built. Known for its very sturdy airframe and forgiving handling, over 16,000 of them were built, including over 10,000 variants in support of the military. Over 400 DC-3s remained in use as of 1998 [37]. Renamed the C-47 for military use, the DC-3 flew during WWII, the Cold War, and in Vietnam as a paratrooper and cargo plane, as well as pulling gliders. The DC-3 is considered one of the most successful planes in aviation history [7], and many commercial planes today are based off the DC-3 design [11]. It could carry 14 to 28 passengers (depending on if it had beds or seats for passengers) or 1,244 cubic feet of cargo weighing about 12,000 pounds, which made it a suitable aircraft to compare to the CBY-3 [9, 8, 10].



Figure 2: Image of Douglas DC-3 [38] © David P. Henderson



## 2.3 Aircraft Performance Metrics

### 2.3.1 Aircraft Historical Data Comparison

Because both the CBY-3 and the DC-3 were designed to be transport aircraft during roughly the same time period, some of the collected experimental data from original flight tests was useful to compare. This data, from a CBY-3 evaluation by the Fairchild Stratos Corporation [26] and from various reports on the DC-3 (specific references cited in the table), is listed in Table 3. The CBY-3 was significantly heavier than the DC-3 but was only slightly slower at cruise condition. The rate of climb for both aircraft was similar but drops drastically for the CBY-3 with one engine running compared to the DC-3 with one engine running. A big advantage of the CBY-3 was the short takeoff distance relative to the takeoff distance of the DC-3. However, both aircraft are able to fly approximately the same distance without refueling. They also have similar engines; the CBY-3 used two Pratt & Whitney Twin Wasp R-2000 (2SD13-G) 2-Row radial engines [5, 13], and the DC-3 used two Pratt & Whitney Twin Wasp R-1830-90C (R-1830-S3C4-G), 2-Row, Radial 14 Engines [10, 14]. All the values listed in Table 3 are measurements used to provide a preliminary comparison of practical abilities of each aircraft.

Table 3: Aircraft Performance Characteristics from Experimental Data

	<b>CBY-3</b>	<b>DC-3</b>
Empty Weight	20,850 lbs [26]	17,000 lbs [8]
Max Weight	32,200 lbs [26]	26,200 lbs [25]
Cruising Speed	193 mph [26]	207 mph [25]
Max level flight speed	229 mph [26]	230 mph [12]
Rate of Climb	1,035 ft/min [26]	1,050 ft/min [9]
Rate of Climb with one engine	51 ft/min [26]	375 ft/min [9]
Takeoff Distance	650 ft [26]	900 ft [9]
Range	1,200 miles [5]	1,300 miles [9]
Rated Thrust per Engine	1,081 kW [13]	895 kW [14]

### 2.3.2 Aircraft Performance Calculations

The data we aimed to collect from the computational fluid dynamics simulations was the vertical and horizontal forces on the aircraft at different angles of attack. The angle of attack is often defined as the angle between the velocity vector of the airflow and the chord line, or centerline, of the airfoil [17]. For our simulations, the angle of attack was defined as the angle

between the velocity vector and the chord line of the fuselage, which acted as the centerline of the entire aircraft. Generally, the lift and drag forces acting on the aircraft are always parallel and perpendicular, respectively, to the flight path of the aircraft, as shown in Figure 3 [15, 17]. Therefore, the lift describes the total upward force, and the drag describes the total force in the direction opposite to the velocity vector. It is important to note that at an angle of attack of zero degrees it is assumed that the lift acts directly against the weight of the aircraft and the drag acts directly against the thrust. All the equations presented in this section are only applicable for steady-level flight conditions. Steady-level flight assumes that the angle of attack is zero, and the velocity of the aircraft is not changing [17].

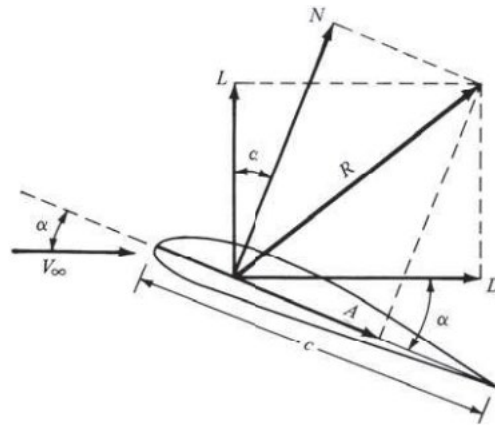


Figure 3: Forces acting on an airfoil [17] © McGraw-Hill Education, 2017

The lift and drag forces can vary significantly based on the flight conditions present, such as air flow velocity and altitude, so comparing the values of these forces directly is not very meaningful. It is more common to compare the lift and drag coefficients, defined in Equations 2.1 and 2.3, respectively. Based on the literature describing CFD simulations of aircraft and aircraft wings [19, 20, 22, 27] we determined that the most important performance metrics are the lift and drag coefficients. These are non-dimensional values representing the lift or drag of an aircraft at specific flight conditions for the aircraft's wing area. According to the classical Prandtl lifting-line theory, lift coefficient varies linearly with the angle of attack at angles below the stall angle [17]. At stall, flow separation occurs, and lift decreases drastically, so the maximum lift coefficient correlates to an angle of attack just below the stall angle. To find the stall angle for a specific aircraft, tests need to be run at many angles of attack. It is also useful to plot the variation of the

drag coefficient as the lift coefficient changes, which is called the drag polar, and can also be described by Equation 2.4 re-arranged to solve for  $C_D$  [17].

Using the lift forces evaluated through CFD, Equation 2.1 can be used to find lift coefficient for each tested angle of attack (test cases discussed in further detail in section 5.1.1) [17],

$$C_L = \frac{L}{\frac{1}{2}\rho V^2 S} = \frac{L}{q S} \quad (2.1)$$

Where  $\rho$  is the density at altitude,  $V$  is the airspeed,  $S$  is the wing area, and  $q$  is defined as,

$$q = \frac{1}{2}\rho V^2 \quad (2.2)$$

Similarly for the drag coefficient,

$$C_D = \frac{D}{q S} \quad (2.3)$$

The drag coefficient can be separated into two components, the induced drag, and the parasitic drag. The induced drag is caused by the lift force and the parasitic drag is due to skin friction and pressure from flow separation around the aircraft [17]. The parasitic drag coefficient is also known as the drag coefficient at zero lift, defined as [15],

$$C_{D_0} = C_D - \frac{C_L^2}{\pi AR e} \quad (2.4)$$

Where  $AR$  is the aspect ratio of the wing, and  $e$  is the Oswald efficiency factor [15]. Equation 2.4 below is the definition of the aspect ratio [17],

$$AR = \frac{b^2}{S} \quad (2.5)$$

Where  $b$  is the wingspan [17].

An important parameter to evaluate for aircraft performance calculations is the aforementioned Oswald efficiency factor,  $e$ . This factor is a measure of how elliptical the lift

distribution is from wing tip to wing tip, and is always between 0 and 1. For an elliptical lift distribution, which represents an ideal distribution, the lift force is strongest in the center of the aircraft, between the wings, and weakest at the wing tips. The magnitude of the lift force also varies in a way that, if represented from a front view, resembles the shape of an ellipse, depicted in Figure 4. If the lift force distribution is a perfect ellipse, the Oswald efficiency factor would be 1 [15]. The Oswald efficiency factor is usually a value between 0.7 and 0.85. The exact value is primarily a function of the complex geometry of the wings, but also accounts for the lift provided by the rest of the aircraft, including the fuselage [17].

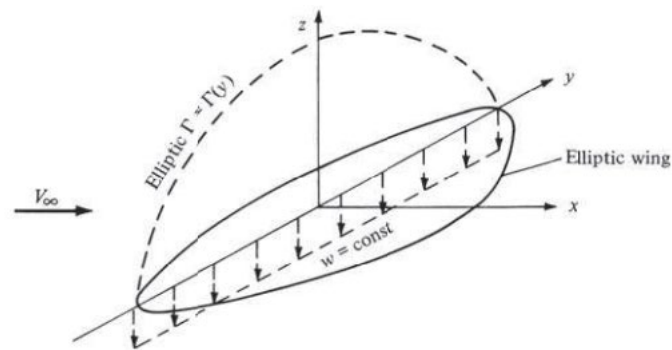


Figure 4: Representation of elliptical lift force distribution on elliptical wings. The curved dotted line represents the lift distribution. [17] © McGraw-Hill Education

Models have been created from experimental data to approximate a value for  $e$  based on the aspect ratio,  $AR$ , and taper ratio (the chord length of the wing tip divided by the chord length of the wing root) [17]. However, this only results in approximate values for  $e$  for aspect ratios of 4, 6, 8, and 10, so interpolating would result in a quite imprecise value for  $e$  [17].

It is also possible to estimate  $e$ , as well as the drag coefficient at zero lift, using the required power of the aircraft as well as the propeller efficiency. This is also derived from experimental flight data of various typical aircraft. However, the propeller efficiency of the CBY-3 is unknown, so we were unable to use this method [15].

Another method for determining the Oswald Efficiency Factor is to start with a rough approximation based on aspect ratio and taper ratio, then correct it to account for influence from the fuselage, parasitic drag, and Mach number [23]. However, these corrections required the diameter of the fuselage, so again a cylindrical fuselage is assumed. The authors of this method provide typical values for the fuselage diameter for many types of aircraft, but the CBY-3 doesn't

fit into typical categories because of its lifting fuselage [23]. Perhaps, given more time, we could have determined an equivalent diameter for the CBY-3 and cross-checked the result with other methods to make sure the calculated value for  $e$  was accurate, but due to time constraints, we chose not to apply this method.

Because of the complexity or lack of information for the previously described methods for finding Oswald efficiency factor, we decided to use the following curve-fit correlation derived from collected experimental data [16],

$$e = 1.78(1 - 0.045 AR^{0.68}) - 0.64 \quad (2.6)$$

Equation 2.6 has been used by other groups investigating aerodynamic performance of aircraft [16, 17, 31] and is considered a good approximation for  $e$  [17, 31]. Because the DC-3 is a widely known aircraft and DC-3 specifications are readily available, the Oswald Efficiency Factor of the DC-3 is reported in the literature as 0.75 [23]. But because this information is not available for the CBY-3, we used Equation 2.5 to approximate  $e$  for both the CBY-3 and DC-3 for consistency.

Once a value for Oswald efficiency factor is determined, Equation 2.4 can be used to find the drag coefficient at zero lift. Then, the maximum lift-to-drag ratio can be found using Equation 2.7,

$$L/D|_{max} = 2 \sqrt{\frac{C_{D_0}}{(\pi AR e)}} \quad (2.7)$$

The maximum lift-to-drag ratio is also a useful metric to compare aircraft since the higher the lift-to-drag, the higher the efficiency of the design [19].

The lift and drag coefficients, as well as the lift-to-drag ratio are the predominant values that influence our conclusions for this project. These values provide an accurate basis for comparison of the aerodynamic efficiency of the CBY-3 and the DC-3. However, the performance of the aircraft can be described using other characteristics which can be calculated from the data collected. These characteristics and calculations are listed below.

Lift coefficient corresponding to the conditions where the lift-to-drag ratio is maximized,

$$C_L|_{L/D_{max}} = \sqrt{C_{D_0}(\pi AR e)} \quad (2.8)$$

The minimum total drag at level flight,

$$D_{min} = 2W \sqrt{\frac{C_{D_0}}{(\pi AR e)}} \quad (2.9)$$

Drag coefficient corresponding to conditions where drag is minimized,

$$C_{D_{min}} = \frac{D_{min}}{q S} \quad (2.10)$$

Airspeed where total drag is minimized,

$$V|_{D_{min}} = \sqrt{\frac{2W}{\rho S}} \sqrt[4]{\frac{1}{(\pi AR e) C_{D_0}}} \quad (2.11)$$

Minimum thrust required for steady-level flight,

$$T_{req} = q S C_{D_0} + \frac{k S}{q} \left(\frac{W}{S}\right)^2 \quad (2.12)$$

Where  $k$  is defined below,

$$k = \frac{4}{3} \frac{1}{\pi e AR'} \quad (2.13)$$

Minimum power required for steady-level flight,

$$P_{req} = \frac{1}{2} \rho V^3 S C_{D_0} + \frac{1}{(\pi AR e)} * \frac{2W^2}{\rho V S} \quad (2.14)$$

Lift coefficient corresponding to conditions where required power is minimized,

$$C_L|_{P_{req_{min}}} = \sqrt{3(\pi AR e)C_{D_0}} = \sqrt{3} * C_L|_{L/D_{max}} \quad (2.15)$$

Airspeed where required power is minimized,

$$V|_{P_{req_{min}}} = \frac{1}{\sqrt[4]{3}} V|_{D_{min}} \quad (2.16)$$

## 3 Analysis Tools and Methods

### 3.1 SolidWorks

SolidWorks, which was developed by Dassault Systèmes in Vélizy-Villacoublay, France is a computer aided design program used for solid modeling of three dimensional (3D) objects. It is a widely available and used program for many different applications in education and engineering [36].

In this project, SolidWorks was used to construct the solid model of the CBY-3 that would be used to conduct the aerodynamic analysis. Since the CBY-3 is a one-of-a-kind aircraft, and much less known than the DC-3, a solid model of the aircraft had to be created from scratch. We were not able to locate any online sources for a solid model and therefore had to generate one for the study. The methodology for this is documented in Section 4.

### 3.2 Excel Calculator for Aircraft Performance Parameters

Microsoft Excel was used to perform the aircraft performance calculations described in Section 2.3. We chose Excel because it can easily organize large amounts of data and copy equations for multiple cases. Excel also has the capability to quickly generate tables and graphs to analyze data [35].

For our purposes, we created an excel spreadsheet that would take aircraft parameters, flight conditions, and the forces calculated by the CFD simulation as inputs, and then it would perform all the calculations presented in Section 2.3. From there, it was very simple to create the tables and graphs to present our results.



### 3.3 Ansys Fluent

We decided that the aerodynamic analysis of the CBY-3 would be conducted using computational fluid dynamics, or CFD, implemented with the Ansys Fluent software. This program is very accessible and has extensive support available at WPI. Ansys Fluent also has a wide variety of programs that it combines in its *Workbench*. In the *Workbench*, Ansys provides the functionality to couple different tasks and programs, which allows for a very smooth workflow and the ability to make small changes without having to redo simple but time-consuming work.

Ansys manages every step of the CFD solution process, starting with the generation of the mesh. Ansys Fluent's meshing process involves using unstructured meshes, also known as unstructured grids or irregular grids, which greatly enhances the quality and flexibility of the mesh. In addition, it is also capable of generating meshes with a high level of geometric complexity. This is accomplished by having the mesh generation work with a large variety of basic geometric shapes [29]. In this project, this was a critical capability, due to the complex, rounded shapes on the aircraft, and importance of the geometry to the results.

Fluent provides a large multitude of solution settings, which allow for a very wide range of simulation customization and personalization for specific projects. One of the most important is the use of either the pressure-based or density-based solvers. According to the Ansys User Guide, it is recommended that one use the pressure-based solver for incompressible flows, or weak compressible flows. A common assumption in aeronautics is that flows with a velocity below Mach 0.3 are to be considered as incompressible, which would most certainly be the case for the aircraft in this study [18]. Although the speed of sound changes depending on the air temperature, it is reasonable to assume that the speed of sound would be close to 340 m/s during the assumed flight conditions of the aircraft [18]. The speed of sound for an ideal gas is given by Equation 3.1, in which  $\gamma$  is the ratio of specific heats of the gas,  $R$  is the specific gas constant, and  $T$  is the temperature in Kelvin [18]:

$$c = \sqrt{\gamma R T} \quad (3.1)$$

Given that all the aircraft velocities we consider are less than 100 meters per second or 224 miles per hour, it was clear that we would be using the pressure-based solver.

To solve for the simulated flows, Fluent solves a series of nonlinear differential equations for the conservation of mass and momentum. These equations, for a viscous, incompressible, homogeneous flow are referred to as the Navier-Stokes equations. These four equations, as implemented in Fluent, are given by Equations 3.2 – 3.5.

*Table 4* defines the variables used in the equations.

Conservation of Mass (Continuity):

$$\frac{\partial \rho}{\partial t} + \frac{\partial(\rho u)}{\partial x} + \frac{\partial(\rho v)}{\partial y} + \frac{\partial(\rho w)}{\partial z} = 0 \quad (3.2)$$

Conservation of Momentum (X Velocity):

$$\frac{\partial(\rho u)}{\partial t} + \frac{\partial(\rho u^2)}{\partial x} + \frac{\partial(\rho uv)}{\partial y} + \frac{\partial(\rho uw)}{\partial z} = -\frac{\partial p}{\partial x} + \frac{1}{Re} \left[ \frac{\partial \tau_{xx}}{\partial x} + \frac{\partial \tau_{xy}}{\partial y} + \frac{\partial \tau_{xz}}{\partial z} \right] \quad (3.3)$$

Conservation of Momentum (Y Velocity):

$$\frac{\partial(\rho v)}{\partial t} + \frac{\partial(\rho uv)}{\partial x} + \frac{\partial(\rho v^2)}{\partial y} + \frac{\partial(\rho vw)}{\partial z} = -\frac{\partial p}{\partial y} + \frac{1}{Re} \left[ \frac{\partial \tau_{xy}}{\partial x} + \frac{\partial \tau_{yy}}{\partial y} + \frac{\partial \tau_{yz}}{\partial z} \right] \quad (3.4)$$

Conservation of Momentum (Z Velocity):

$$\frac{\partial(\rho w)}{\partial t} + \frac{\partial(\rho uw)}{\partial x} + \frac{\partial(\rho vw)}{\partial y} + \frac{\partial(\rho w^2)}{\partial z} = -\frac{\partial p}{\partial z} + \frac{1}{Re} \left[ \frac{\partial \tau_{xz}}{\partial x} + \frac{\partial \tau_{yz}}{\partial y} + \frac{\partial \tau_{zz}}{\partial z} \right] \quad (3.5)$$

Table 4: Navier-Stokes Equations Variables

Property	Position	Velocity	Time	Pressure	Density	Stress	Reynolds Number
Variable	$x, y, z$	$u, v, w$	$t$	$p$	$\rho$	$\tau$	$Re$
Unit	$m$	$m/s$	$s$	$Pa$	$kg/m^3$	$Pa$	

A part of the classic definition of the Navier-Stokes equations is the Conservation of Energy equation. This equation is used to solve for the changes in flow characteristics caused by

compressibility effects. However, due to the incompressibility assumption stated before, this equation was not part of our simulations. In addition to the four equations used to describe the conservation of mass and momentum, a turbulence model is also included in the calculations. Due to the viscous effects present in the flow, caused by the interaction of the aircraft and the air flow, not including this aspect would have a large negative impact on the total lift and drag calculated in the simulation [18]. There are many choices available when selecting how to simulate turbulence, and it can also be difficult to deduce which ones are better for different conditions [29]. For all the simulations run in this project, the turbulence model that was chosen was the  $k - \omega$  shear-stress transport (SST) model.

The  $k - \omega$  SST model is described as “more accurate and reliable for a wider class of flows (e.g., adverse pressure gradient flows, airfoils, transonic shock waves) than the standard  $k - \omega$  model” in the Ansys User guide [29]. It can model different interactions of the flow depending on the local proximity to walls, which both increases accuracy and reduces calculation time. In the flow calculation, this is represented by an additional two non-linear differential equations done for each iteration, shown in Equations 3.6 and 3.7. Table 5 defines the terms in these equations.

$$\frac{\partial}{\partial t}(\rho k) + \frac{\partial}{\partial x_i}(\rho k u_i) = \frac{\partial}{\partial x_j} \left( \Gamma_k \frac{\partial k}{\partial x_j} \right) + \tilde{G}_k - Y_k + S_k \quad (3.6)$$

$$\frac{\partial}{\partial t}(\rho \omega) + \frac{\partial}{\partial x_i}(\rho \omega u_i) = \frac{\partial}{\partial x_j} \left( \Gamma_\omega \frac{\partial \omega}{\partial x_j} \right) + G_\omega - Y_\omega + D_\omega + S_\omega \quad (3.7)$$

Table 5: k- $\omega$  SST Equation Variables

Property	Generation of Turbulence Kinetic Energy	Generation of $\omega$	Effective Diffusivity of $k$	Effective Diffusivity of $\omega$	Dissipation of $k$	Dissipation of $\omega$
Variable	$\tilde{G}_k$	$G_\omega$	$\Gamma_k$	$\Gamma_\omega$	$Y_k$	$Y_\omega$
Property	Cross Diffusion Term	User Defined $k$ Source	User Defined $\omega$ Source			
Variable	$D_\omega$	$S_k$	$S_\omega$			

With the equations defined, Fluent must solve for these six non-linear differential equations. This is accomplished by first starting with an initial guess for each of the solutions, and then iterating on those solutions a number of times. For each iteration, the solver compares the current solution with the previous one and classifies the difference between the two as the residual value. This residual value determines how many iterations are required for the solution to converge. Convergence is defined as having been reached when the residual value for each equation is smaller than a user-determined value; this means that the solver is calculating the same value between two iterations. Figure 5 from Reference 29 shows the logic between each iteration, and how the solver works towards convergence.

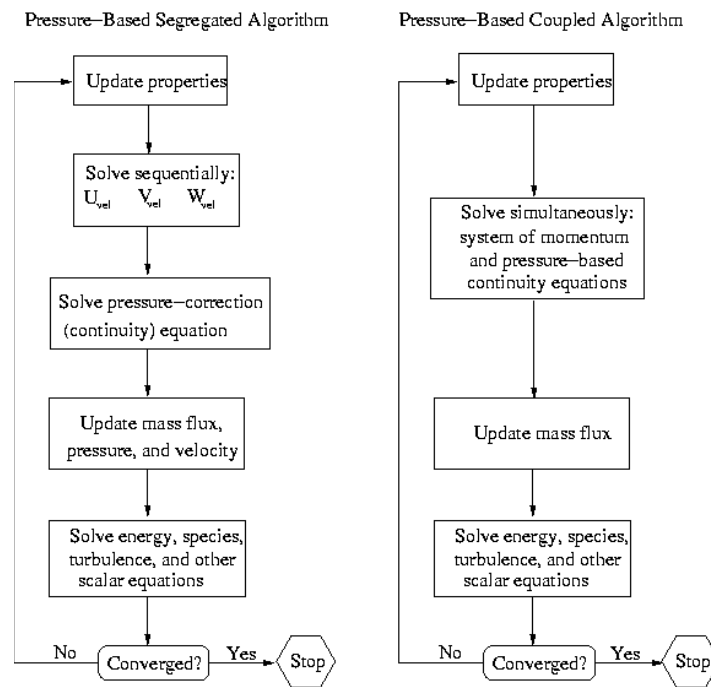


Figure 5: Overview of the Pressure-Based Solution Methods [29]. © Ansys, Inc. 2009

In Figure 5, the two versions of the solver correspond to a segregated solver, and a coupled solver. The key difference between the two is that the coupled solver finds a solution for the velocity equations at the same time that it solves the continuity equation. By doing this, it reduces the steps required to solve, which decreases the amount of time each iteration requires. However, this process requires between 150-200% more memory than the segregated solver, which would necessitate the use of a much more powerful computer. In the cases run during this project, the segregated solver was used.

In addition to the standard hybrid initialization that is used to obtain the first solution for the solver, Full Multigrid (FMG) initialization was utilized. FMG initialization is an advanced form of initialization that helps accelerate the rate of convergence by calculating a much more advanced initial solution [29]. The solver is able to work through most of the coarse corrections that the solver would have to go through in a notably shorter amount of time, which can reduce the amount of time a complex solution would need. Figure 6 shows the process that FMG initialization goes through to compute the initial solution. In this Figure, the horizontal axis represents the number of cycles executed in the initialization process, and the vertical axis represents the coarseness of the corrections being made. What Figure 6 represents is as FMG initialization advances through levels, it starts by only making coarse corrections, and works towards making finer corrections in the initial guess.

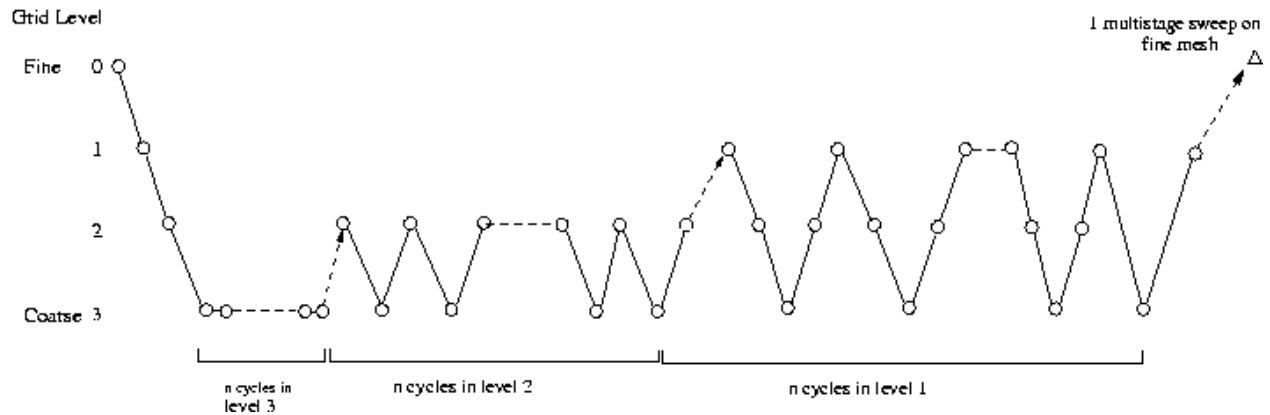


Figure 6: FMG Initialization [29]. ©Ansys Inc. 2009

For further information on any topic presented in this section, the reader is referred to the Ansys Fluent User Guide. This guide was the source of all the information above and goes much further into detail about all the mentioned methods, as well as all the other options and capabilities of Ansys Fluent.

## 4 Methodology to Create a Solid Model of the CBY-3 Loadmaster

### 4.1 3D Laser Scanning to Create a Solid Model

When initially determining how we could generate the 3D model of the CBY-3, we first considered scanning a wind tunnel model of the aircraft with a device that would generate a digital “solid” object. This object could then be imported into SolidWorks. This idea seemed appealing, as it would allow for a quick generation of the model, as well as being accurate to the design of the aircraft. However, there were complications that eventually caused us to not use this approach.

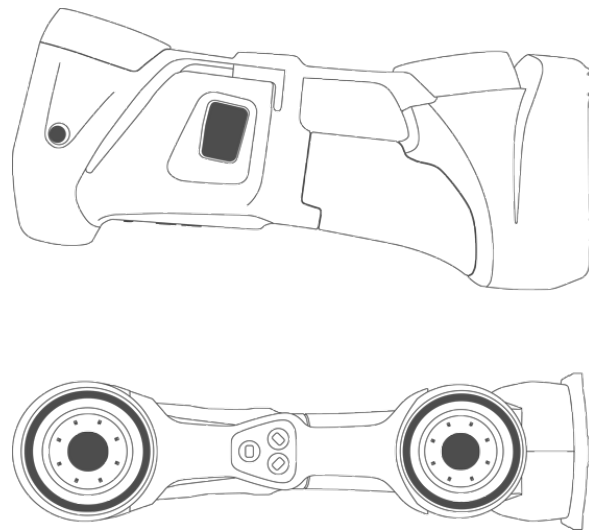


Figure 7: Creaform HandySCAN 3D Silver [24]. © Creaform 2022

One reason we decided against this approach was due to the budget limits of the project, and the potential expense of a high-quality scanner. The scanner shown in Figure 7, the Creaform HandySCAN 3D Silver Series was quoted to cost in the range of \$20,000 to \$30,000, which was far outside our budget. Scanning the aircraft or a model of the aircraft also proved to have challenges of its own, such as how to maintain accuracy, and how to make surfaces more reflective without damaging original materials. However, we did decide that there could be an application for this, when examining small individual components, such as wing brackets or switches. For further information on this application, please refer to the MQP Report “Structural Design Analysis of the Burnelli CBY-3 Loadmaster” [34].

## 4.2 Creating a Solid Model from 2D Printed Plans: Preparation

A second approach, which we eventually chose to pursue, was to use original design documents to create a model of the aircraft. Since scanning the entire aircraft was not a viable option, it was clear that this was the approach we would be taking.

We researched methods of solid model generation from original 2D print plans, but unfortunately did not find any academic publications on the subject. Although there did not appear to be any significant industrial or commercial research into this concept, we did identify some groups that had attempted similar approaches. For example, miniature model makers had published many 3D printed models of aircraft, including almost everything from the birth of flight to the modern era. Printing these 3D models would have required creation of a solid model, the exact problem we were trying to solve. Unfortunately, those modelers we reached out to did not respond.

To start developing the model, original blueprints were first collected and assessed to identify what might be most valuable. We decided that while particular technical documents would be very helpful for certain specific parts of the model, such as the wing or tail construction, one document we identified with the help of the NEAM staff would provide the 2D views needed to create the initial sketches of each major component of the aircraft, i.e., wings, fuselage, tail booms, and stabilizers. This document was the original patent file for the Loadmaster II, Cargo Version by the Burnelli Avionics Corporation from 1945, shown in Figure 8 [NA1]. This document was chosen due to its accurate display of the whole aircraft, which would be invaluable in getting proportions and general geometry of the aircraft correct. The inclusion of many dimensions in the drawing would also enable a high degree of fidelity to the actual, as-built aircraft. The original file, as well as the three individual views, can be seen in Figures 8 through 11.

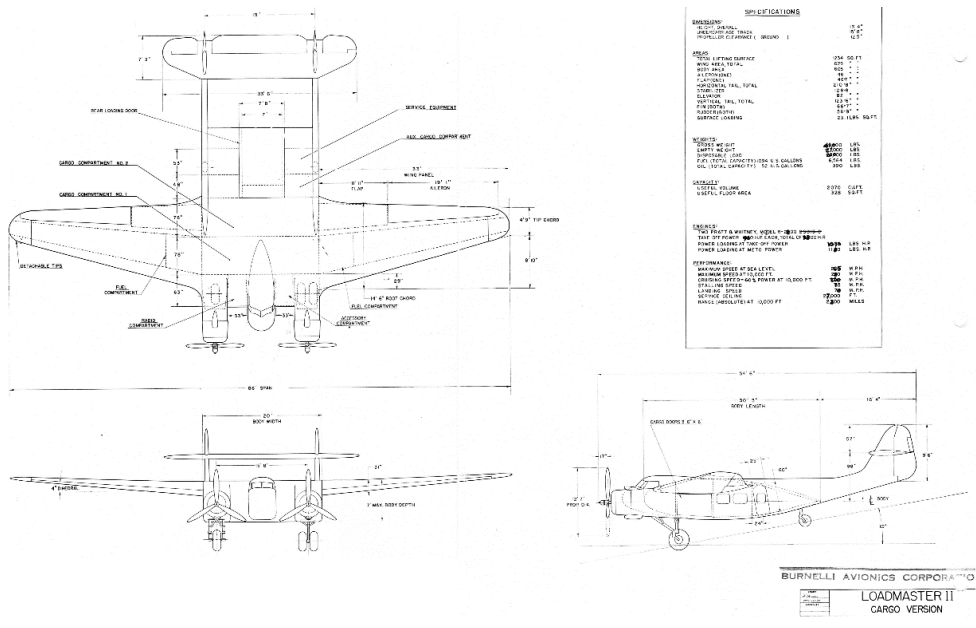


Figure 8: Burnelli Avionics Corporation Loadmaster II [NA1]

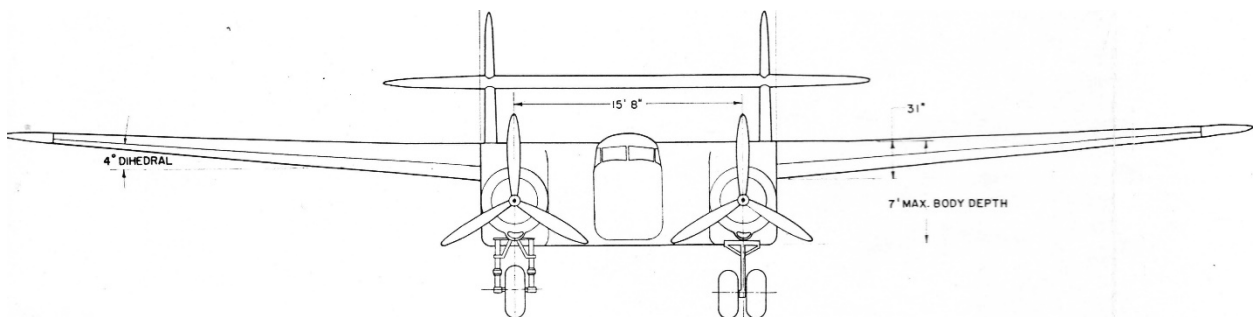


Figure 9: Loadmaster Patent File: Front View [NA1]

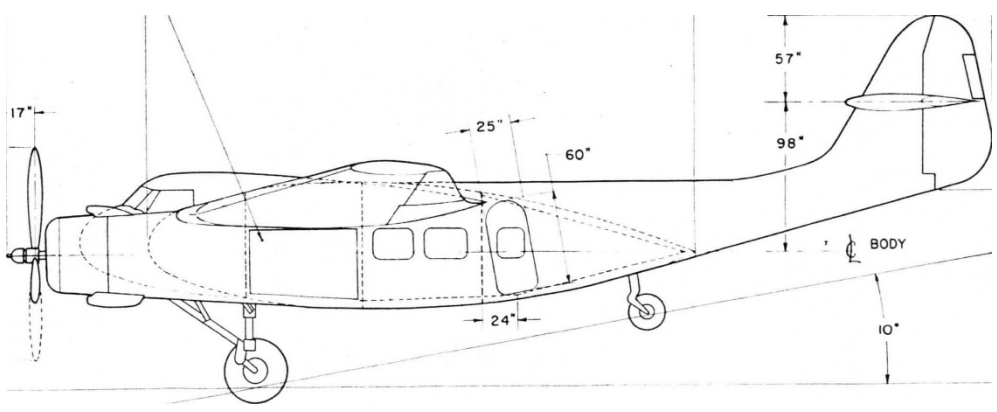


Figure 10: Loadmaster Patent File: Side View [NA1]



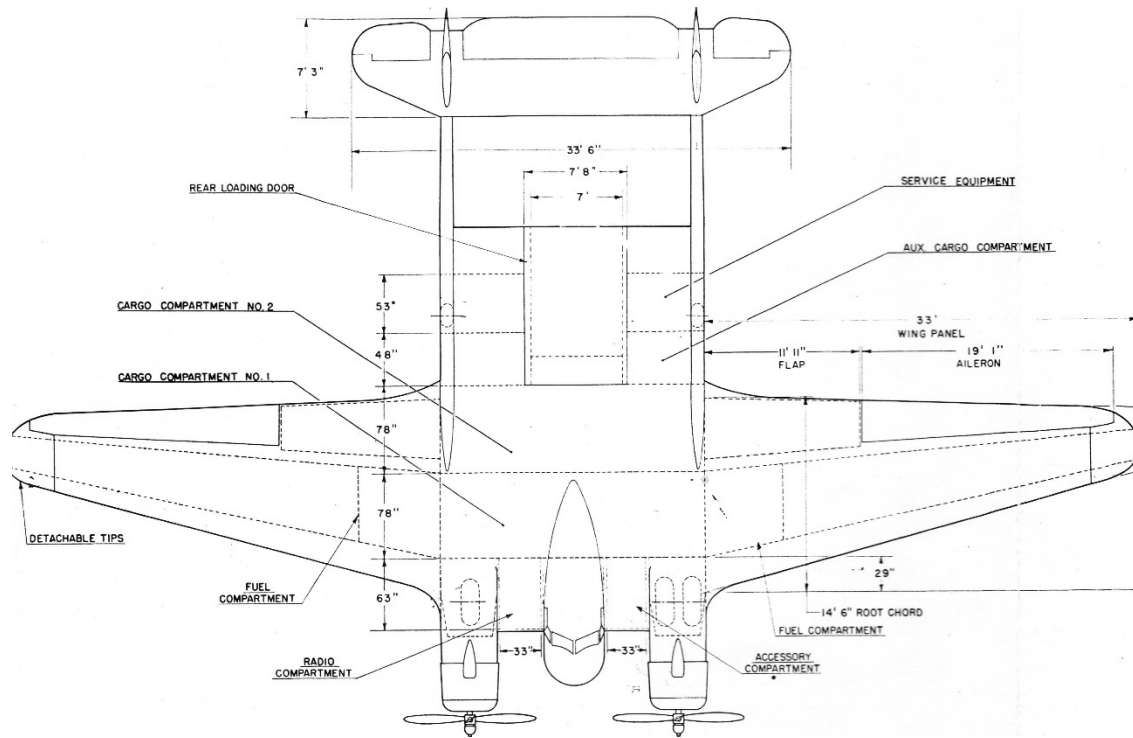


Figure 11: Loadmaster Patent File, Top View [NA1]

For some specific parts of the aircraft other technical documents were consulted. One of these documents was titled Basic Dimensions of the Wing & Spars [NA2]. This document was used due to its large number of provided dimensions for the wing, such as the chord length, camber, and angle of attack of the wing relative to the body. Since these dimensions play a large role in defining the aerodynamics of the aircraft, we found it important to make sure these dimensions were as accurate as possible. This was similarly done for other components of the aircraft, such as the tail booms, the vertical and horizontal stabilizer, the fuselage, and engine cowls. The documents used, as well as a general description of the files, can be found in Section 7.2 and Appendix A.

Once the patent file was scanned and available, it was then separated into the three views of the aircraft and imported into SolidWorks. This was a simple process, as SolidWorks has a function which allows for the insertion of a 2D image anywhere in a part or assembly file. When the images were imported, they were arranged so that the three views were all perpendicular and correctly scaled to the listed dimensions. This setup is shown in Figure 12 and was used as the base file for the entire designing process. This foundation created a method for us to generate the

outline sketches for each aircraft component, as well as a way for us to reference the parts afterwards to judge how well they fit with the design drawings.

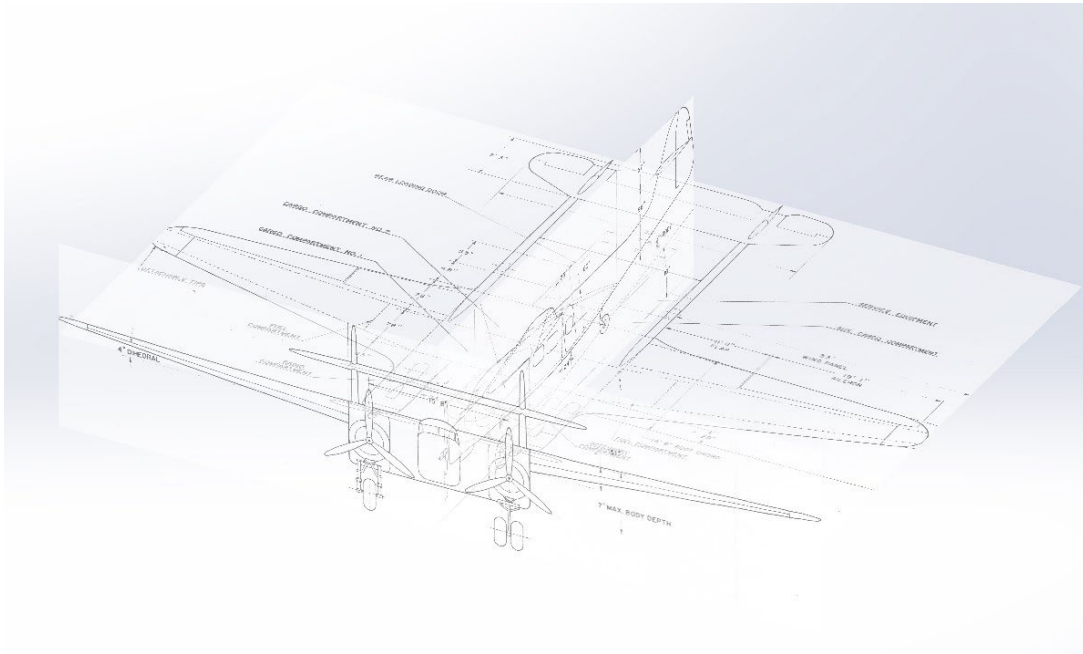


Figure 12: SolidWorks Layout for Loadmaster

### 4.3 Creating a Solid Model from 2D Printed Plans: Generation of 3D Forms

Because the available blueprints for the aircraft were drafted over 70 years ago, not everything was scaled and dimensioned perfectly. Soon after sketching began, we discovered that the aircraft blueprint had some small variations between views. For example, the right view and top view, although both sized based on the total length of the aircraft, produced slightly different dimensions. In addition, some of the components did not line up perfectly between the sketches.

Therefore, we concluded that the best method for creating the model would be to use the blueprint for reference, while relying on the dimensions to properly scale and correct the sketch. The blueprint would provide the geometry of each component, and then the sketch would be adjusted with the correct dimensions, to the extent that the dimensions were provided for each component. In SolidWorks, we started parts by tracing the outlines of components from multiple views. These views were mostly the side and top view, due to them having the majority of details. Then, once we created the general form of the part in two perspectives, any known dimensions were added, and the sketches were aligned. All that was left was to use either a loft or extrude to properly fill in the outline and generate the 3D version of the sketches.

This process ended up being more time consuming than was originally planned. As we had only a limited amount of SolidWorks experience before the start of the project, there were a number of skills we needed to develop in order to build up to a steady work pace. To supplement this, the team took part in a SolidWorks training meeting with Dr. Erica Stultz at WPI, who was very helpful in providing insight into best practices. One suggestion that was very helpful was the prioritization of cross sections in the modeling process. One example of this is clearly shown in the creation of the wing. Although the section of the wing (i.e., a plane normal to the span) close to the body of the fuselage does have varying geometry, most of the wing shape can be accurately described by two airfoils. An early version of this is shown in Figure 13.

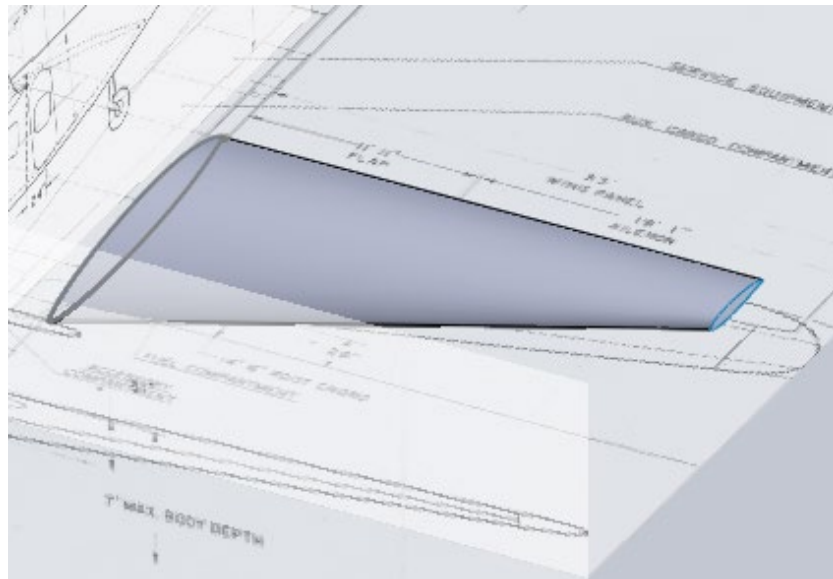


Figure 13: Early Sketch of CBY-3 Wing in SolidWorks

Another good example of a similar process can be seen in the horizontal stabilizer. Parts of the design are simple airfoils with the same airfoil geometry in the spanwise direction. These were created first, to use as reference points. Then, SolidWorks was able to understand that these two objects needed to be connected using a specific guide sketch. In this process, a guide sketch is a simple curve or line that acts as a guide for the connection of two faces. Although this small step required significant preparation and alignment to work correctly, when it was right it worked very well. The mating of two reference airfoils, with the same shape but different sizes, using a guide sketch is shown in Figure 14, with the guide sketch being specifically highlighted in pink.

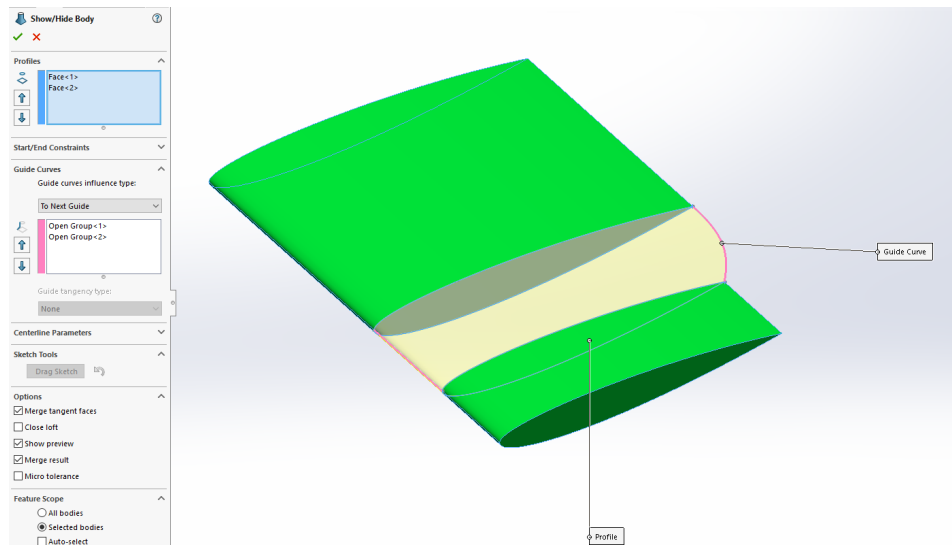


Figure 14: Creation of Horizontal Stabilizer Geometry

It was this general process that allowed us to generate the complex geometry of the CBY-3. In some cases, such as the engine cowls and parts of the nose, there were some dimensions that had to be inferred from the dimensioned drawings available to us. Although this was not very common, there were some parts of the model that were based on large scale geometry and certain known features, rather than specific dimensions provided in a reference. For example, the exact shape and dimensions of the part of the engine cowl that transitions into the fuselage was not known. Based on design drawings that included it, as well as using the actual aircraft as a reference, we were able to estimate the required dimensions.

Because the eventual purpose of the solid model was to enable aerodynamic simulation and analysis, priority in terms of high-fidelity modeling was given to those parts of the aircraft, such as the fuselage, horizontal stabilizer, tail booms and wings, that most affect the aerodynamic performance. Other parts of the aircraft that have less impact on aerodynamic performance were not modeled as accurately. The best example of this are the propeller mounts on the engines. Although the detailed geometry and dimensions of the mounts could likely have been measured directly on the aircraft, or identified in a document, we decided to make a simplified model, based on the dimensions of other components nearby. Another example is the internal geometry of the engine, which was highly simplified and estimated. Some aircraft components that were excluded entirely from the model are discussed in Section 4.4.

In Figure 15, one can more clearly see the complex geometry that makes up the front of the aircraft. It is very visible, based on the outlines present, how we defined the geometry, as well as what features were neglected. For instance, the cabin windows were simplified into a smooth shape.

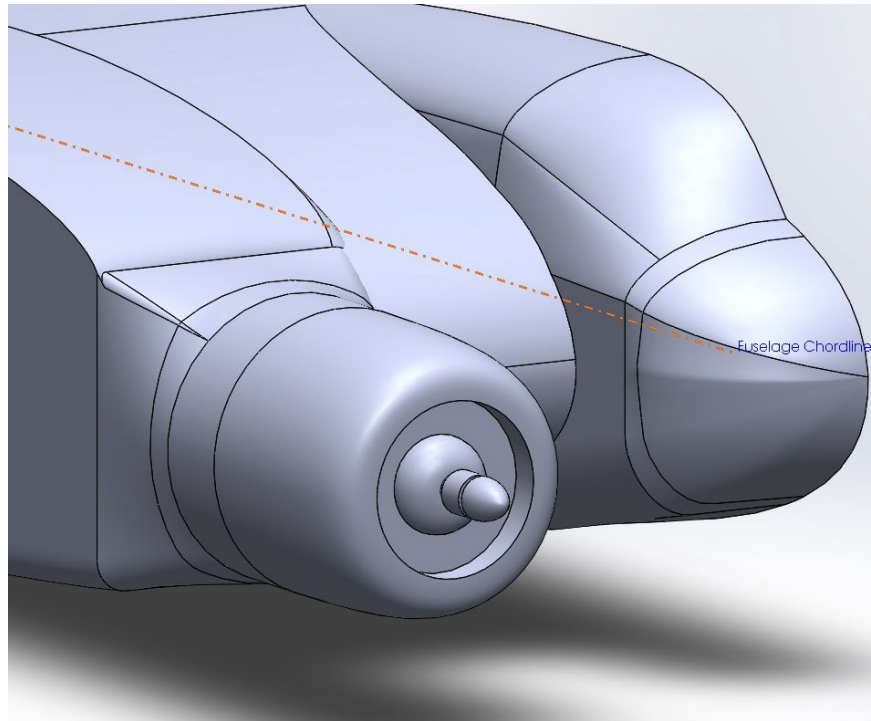


Figure 15: Close-up View of Front of Aircraft

Once all the individual parts were created, including the fuselage, tail, and wing, they were then assembled. At this stage in the process, the model had been defined with specific points where the different parts would connect, which made this process very simple. Once the solid model of the aircraft was assembled, there were some further simplifications made, mostly with the fitting of the top of the wing and the fuselage. At this point, the SolidWorks model of the CBY-3 was complete, and it was ready to be imported into Fluent (Figure 16).

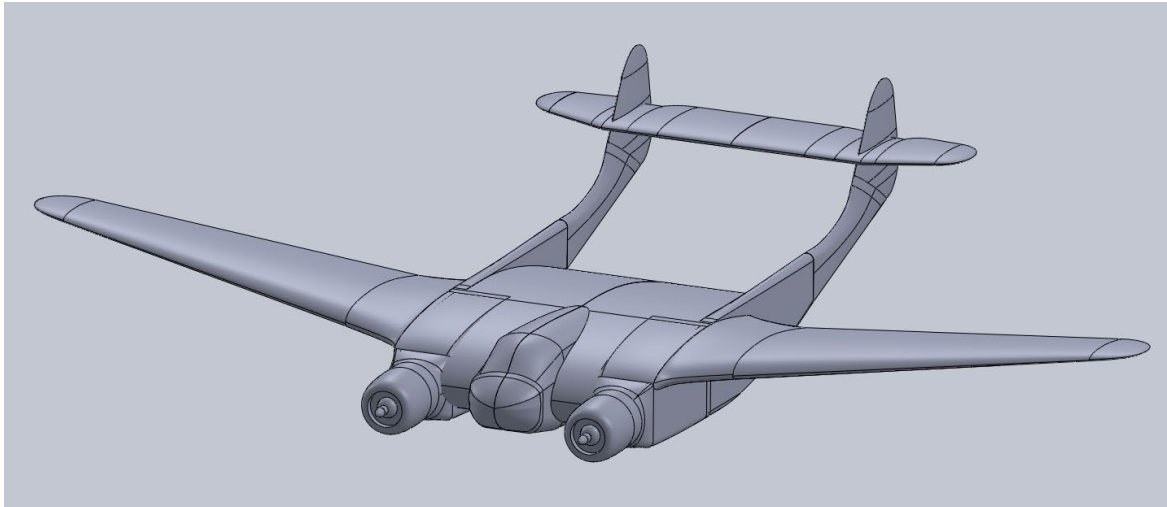


Figure 16: Completed Model of CBY-3 Loadmaster

Appendix B includes a series of screenshots of the completed model with key dimensions displayed. These can be viewed and referenced to the original design documents as a measure of accuracy of the model.

#### 4.4 Excluded Features from Model

There are some features of the aircraft that were excluded from the model of the Loadmaster. These were details that we determined to be insignificant drivers of aerodynamic performance, and therefore did not require modeling. Most obviously is the simplified cabin geometry, and the lack of windows and doors on the fuselage.

As well as aesthetics, other components that were not included were the propellers and the extrusions found on the tail structure. The propellers were not included in the model due to the complexity they would add to the simulation without contributing much to the overall performance of the aircraft. The difference caused by not including the propellers in the model would mostly be the lack of the accelerated flow, and therefore a higher pressure, on the sections of the wing behind the engines. This difference was considered to have a negligible effect on the overall aerodynamic parameters of the aircraft.

The geometry corresponding to the intersection of the horizontal and vertical stabilizers, visible in a photo of the actual aircraft in Figure 17, posed a unique challenge. Once we started working closely with the CBY-3's blueprints and design documents, it became obvious that the protruding feature was not included in any of the documents. When we spoke to NEAM staff about



this feature, they stated that it was most likely a design change that was made during the flight-testing period of the aircraft. It was not known exactly what its purpose was, however one NEAM staff member mentioned that it probably helped with the control stability of the CBY-3. We decided that since it most likely did not significantly contribute to the lift or drag of the aircraft, and dimensional information was not readily available in documents, we would not include it on the final model.

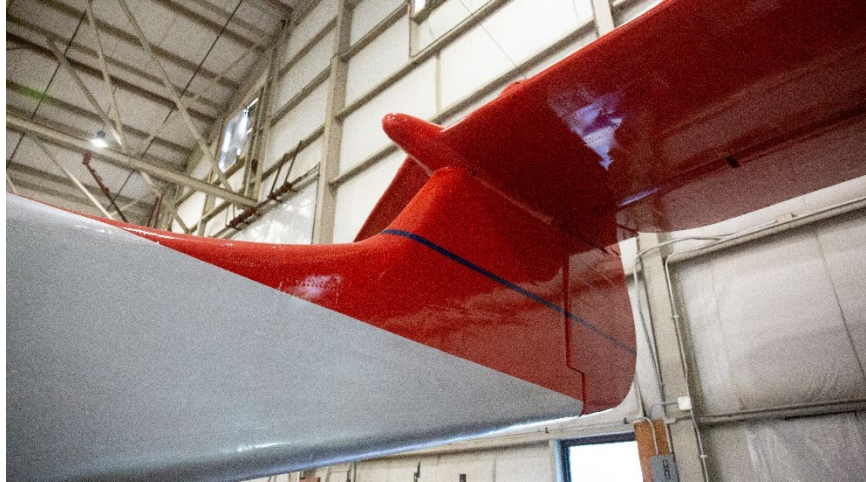


Figure 17: Additional Feature found on Tail Structure of the CBY-3

#### 4.5 Sourcing DC-3 Model for Comparative Analysis

By the time that the CBY-3 model had been completed, it was clear that attempting to follow the same methodology for the DC-3 would result in almost no time to learn, run, and analyze Fluent aerodynamic simulations. Although data on the DC-3 is widely available, and by this point our SolidWorks ability was much more advanced, it still would have consumed a large amount of time. Fortunately, this series of events was anticipated at the beginning of the project, and early on we began research into publicly available CAD models of the DC-3.

The model we chose to use was a SolidWorks model of the DC-3 constructed by Michel Man, that was originally posted on [grabcad.com](http://grabcad.com)<sup>1</sup> on the 28<sup>th</sup> of November 2021 [32]. Although appearing to be a passion project by the maker, the model seemed to reflect the geometry of the DC-3's aerodynamic features well. It was also a 1:1 model of the aircraft, which was the same case for the CBY-3 model. As a check of the model's accuracy, we looked closely at specific

1. [Grabcad.com](http://grabcad.com) is a publicly accessible CAD model database and forum, made to encourage help with collaboration and sharing 3D models [33]

components where complex geometry of the aircraft was expected, such as the wing attachment to the fuselage, the wing tips, and the engine cowls. Most importantly, the airfoil shape and size of the model closely resembled the expected shape of the NACA 2215 airfoil used on the DC-3 [10]. The original model by Michel Man is shown below in Figure 18.

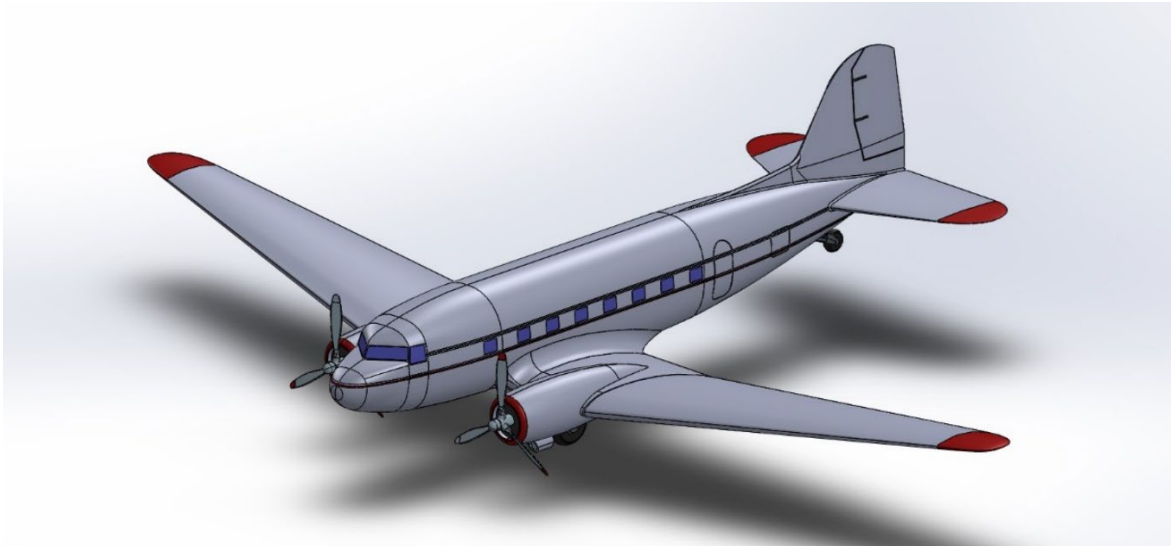


Figure 18: Original Sourced Model of the DC-3 [32]

There were many small details that were also included in the file, such as a very detailed landing gear, propellers, windows, and control surface cutouts. To match the detail quality of the Loadmaster model, we made some simplifications and modifications to the sourced model. These included the filling in of windows, removal of landing gear structure and wheel wells, and filling in of the door and access panel outlines. These changes are shown in Figure 19 and Figure 20.





Figure 19: Simplified DC-3 Model

Although some of these simplifications would not likely have a large effect on the aerodynamics of the aircraft, they did greatly reduce the complexity of the aircraft's geometry. This in turn allowed for a smaller surface meshing of the aircraft once it was imported into Fluent, which reduced file sizes and simulation times. This also allowed for a more reasonable comparison between the two aircraft models.

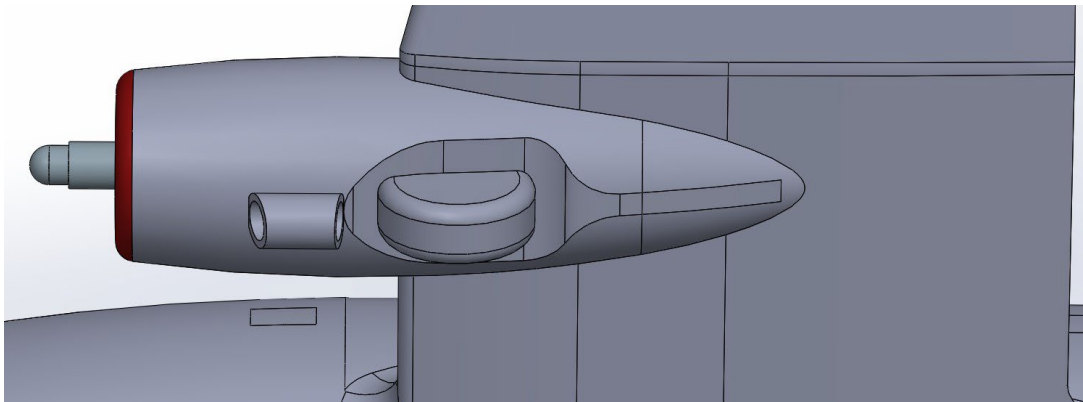


Figure 20: Close-up View of Wheel Well Simplification

## 5 Computational Fluid Dynamics (CFD) Analysis

### 5.1 Problem Description

#### 5.1.1 Test Cases

To begin the investigation of the aerodynamic characteristics, we first decided exactly what aerodynamic characteristics and performance parameters would be calculated. Due to time restrictions, we decided to investigate primarily the flight characteristics of each aircraft in its nominal cruise flight condition, as well as at a set of different angles of attack. The numerical “tests” were also all run at conditions corresponding to sea level. Running tests at multiple different altitudes would necessitate an exponential increase in the number of simulations performed, since at each altitude all the tested angles of attack would need to be evaluated. Because we had to limit the number of test cases, there we were not able to evaluate the absolute ceiling and service ceiling (i.e., the maximum altitude where a positive total vertical force is achievable, and the altitude where the minimum rate of climb achievable is 100 feet per minute, respectively).

For each case, the aircraft are moving at their respective cruising velocities. For the CBY-3 this speed is 193 miles per hour [26], and the cruising speed of the DC-3 is 207 miles per hour [25]. These speeds correspond to the velocity of air moving around the respective aircraft at the different angles of attack. By using one speed for each test case, it would be easier to evaluate the aircraft’s performance at more angles of attack and be able to compare them more accurately. The Reynolds Numbers for these tests were  $9.754 \cdot 10^7$  for the Loadmaster, and  $12.472 \cdot 10^7$  for the DC-3. These values were calculated using the total length of the aircraft, 54.5 feet and 65 feet respectively, as the characteristic length.

The angles of attack that were simulated ranged from -5 degrees to 10 degrees, in increments of 2.5 degrees. By running a total of seven simulations per aircraft, it was possible to verify that the data that is being collected followed expected trends, such as a linear increase in lift coefficient as the angle of attack increases. The angle of attack was defined as the angle between the fuselage centerline or fuselage chord line, and the direction of airflow. This was a specification that was necessary due to a specific design feature of the DC-3. On the DC-3, the wings are mounted to the body with an angle of attack of ~2.5 degrees between the wing chord line and the fuselage centerline. This can be observed on the model of the aircraft used in this study and was confirmed with other design documents. Therefore, we expected that at 0 degrees angle of attack

(i.e., the angle between the air flow vector and the fuselage chord line), the DC-3 would have a large advantage over the CBY-3, since the CBY-3's wing's chord line is parallel to the chord line of the fuselage. One should note that the term chord line was exclusively used when referring to the CBY-3's fuselage, due to its airfoil design. In contrast, the term chord line does not easily apply to the conventional fuselage design of the DC-3. This was a feature specifically pointed out in multiple CBY-3 design documents, that will be discussed further in Section 5.2.

In previous studies comparing aerial vehicles, lift coefficient, drag coefficient, L/D ratio, and weight were compared. Simulations were run on just the wing as well as the entire vehicle at cruising speed with 0 angle of attack for both vehicles being compared [19]. This was done in the interest of validating certain claims, which varied depending on the purpose of each respective study. An example of such a claim was that the CBY-3's unique fuselage design contributed 40% of the total lift force [6]. Because Ansys Fluent calculates and stores data after the completion of a simulation, this data was very easy to access. This specific topic is covered in Section 6.2.

#### 5.1.2 Mesh Sizing

Finding the right size for the mesh was an important step in preparing the simulation. To properly represent the geometry of the aircraft, it was necessary to select a mesh size small enough so that critical details would not be left out. The main concern was with the curvature of the leading edges of the aircraft, since these regions would contain relatively large changes in shape over very small distances. However, if too small of a mesh size was chosen, the mesh file would grow to be excessively large, which would both be difficult to store and access and greatly extend the simulation time. Therefore, a balance had to be found between geometric accuracy and simplicity.

When Fluent generates the surface mesh of the aircraft, it is able to measure the “jaggedness” of the cells by calculating the maximum skewness of the cells. Skewness, in this case, is defined as “the difference between the shape of the cell and the shape of an equilateral cell of equivalent volume” [29]. When generating the volume mesh, it does something very similar by measuring the maximum cell orthogonal quality, which is a measure of how “squished” the cell is [29]. For both aircraft, there were specific requirements for both components that helped ensure that the generated mesh accurately reflected the geometry. The maximum skewness for the surface mesh was limited to a maximum 0.95, and the orthogonal quality to a minimum of 0.1. Both values were determined from the Ansys User Guide, as good requirements for mesh generation [29].

Table 6 and Table 7 show the size limits that were selected for each section of the aircraft. By inputting these minimum and maximum values for the sections, it allowed for total control over the accuracy and complexity of each section. However, there was an effort to have the minimum sizes of each section close to each other, so that the two aircraft models would have a similar level of fidelity. The different sections represented in the mesh sizing are displayed in Figure 21.

Table 6: CBY-3 Mesh Sizing

CBY-3 Section	Minimum Cell Size ( <i>in</i> )	Maximum Cell Size ( <i>in</i> )
Body	6	24
Tail	2	24
Wing	2	12
Body Trailing Edge	0.5	2

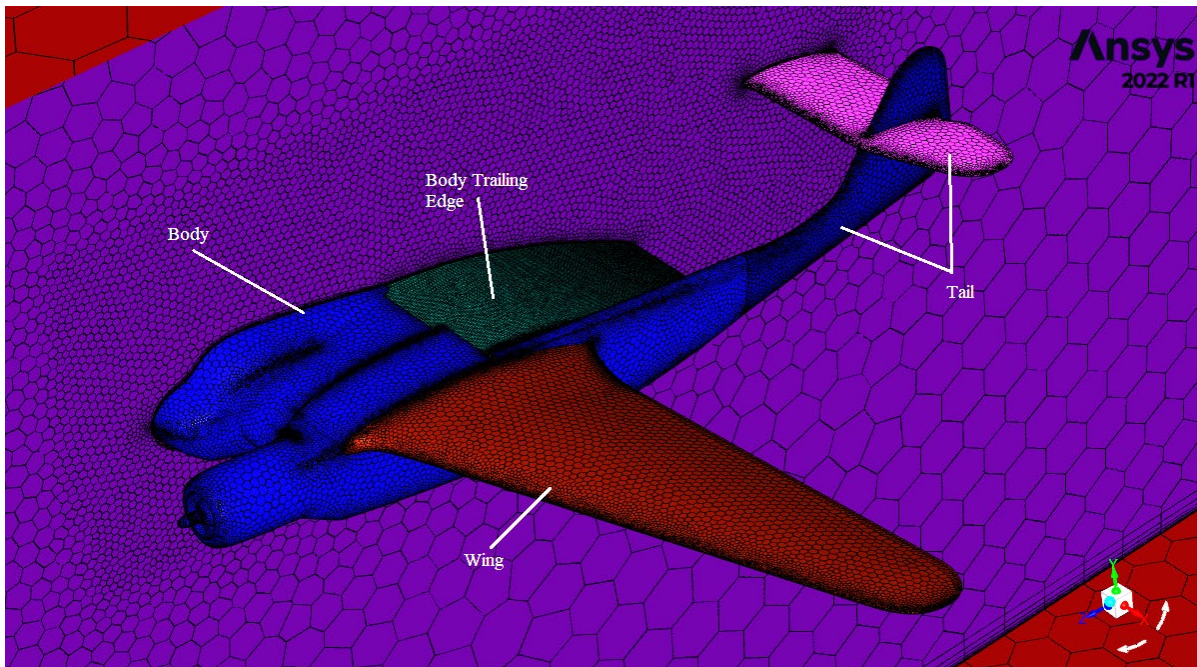


Figure 21: CBY-3 Surface Mesh Generation with Labeled Components

Table 7: DC-3 Mesh Sizing

DC-3 Section	Minimum Cell Size ( <i>in</i> )	Maximum Cell Size ( <i>in</i> )
Body	6	12
Tail	2	24
Wing	2	18
Tail Trailing Edge	0.05	0.1

In addition to the surface of the aircraft having a specific mesh resolution, the air around the aircraft was also defined by a mesh with a range of sizes. In these simulations, there were three separate areas of the surrounding air domain that were part of the simulation. There were two areas close to the aircraft, referred to as bodies of influence (BOI). The bodies of influence were given specific mesh sizes, so that in certain areas the air flow would be more accurately calculated, and sharper changes in air properties could be measured. These bodies of influence are shown in Figure 22 and Figure 23. The bodies of influence were not specified with a specific size, as it was created as more of an approximation of areas of high mesh density. In the simulations, the closest body of influence was only slightly larger than the aircraft, and the second body of influence was extended out by approximately eight feet on five of the six faces. The sixth, or rear face of the second body of influence was extended to the far end of the (virtual) wind tunnel, also referred to as the “enclosure”, to accurately model the turbulent flow behind the aircraft.

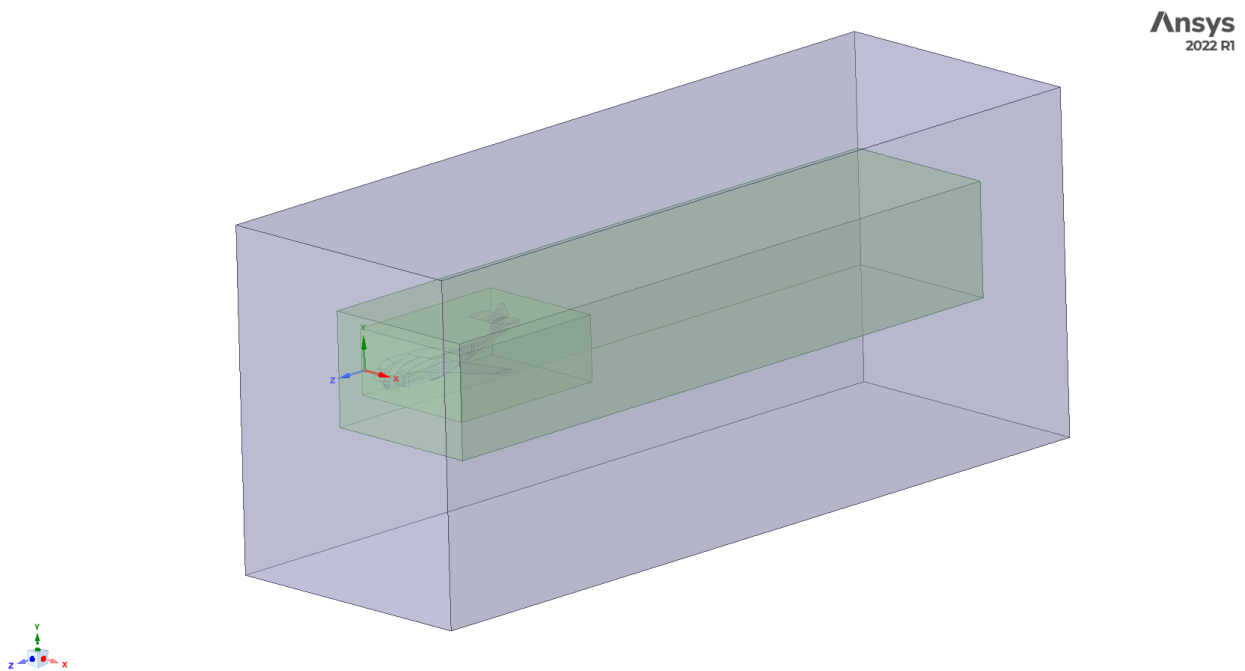


Figure 22: CBY-3 Virtual Wind Tunnel, with Bodies of Influence Visible



Figure 23: Top View of CBY-3 Virtual Wind Tunnel

For both aircraft, the enclosures were given the same sizing parameters. To create the air domains of the simulations, a volume mesh was generated using the surface meshes of the BOIs and aircraft. The volume mesh would be present throughout the air domain, in contrast to a surface mesh, which serves as an infinitely small outline. Those parameters, which include the parameters for the surface mesh and the volume mesh, can be seen in Table 8.

Table 8: Mesh Sizing of Simulation Volume Components

	Target Mesh Size (in)
BOI-near	6
BOI-far	48
Volume Mesh (total)	0.05-102.4

The very large difference in the limits for the volume mesh allowed for the very small details, such as at the areas around the trailing edge of the lifting surfaces, to be modeled accurately, while allowing the large areas in the enclosure to be as vast as possible. Since these were areas of low interest and would have a much more marginal effect on the aerodynamic properties of the aircraft, it was much less important to model. This further reduced the size of the mesh, and greatly reduced the time required for each simulation. Figure 24 and Figure 25 show the volume meshing of the CBY-3 simulation. This volume mesh was very similar in each simulation.



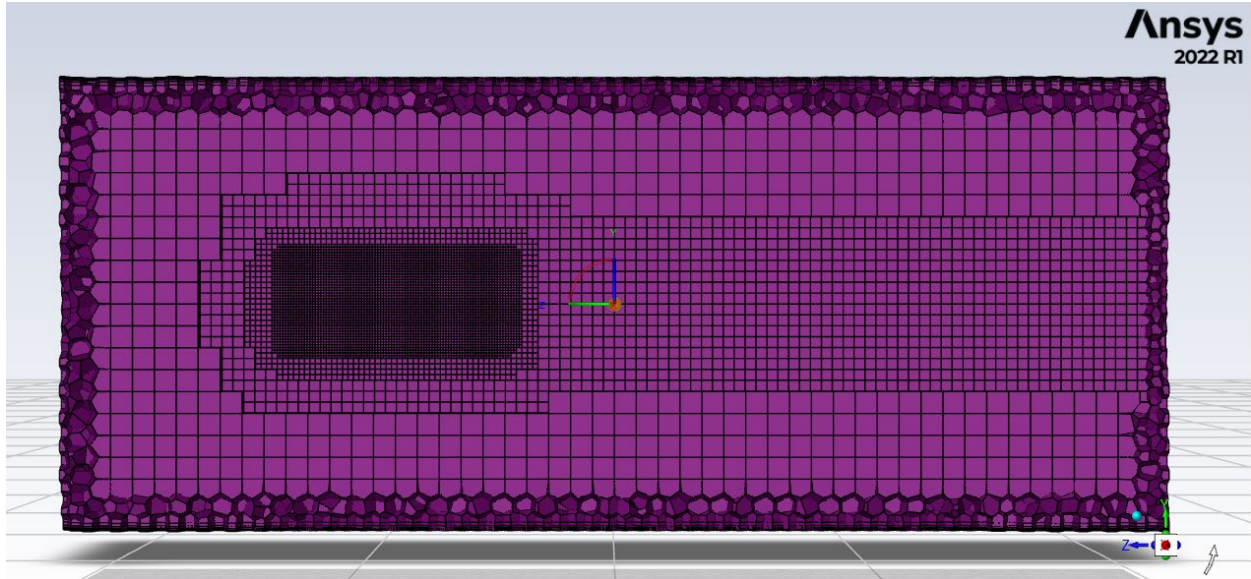


Figure 24: Volume Mesh of Bodies of Influence

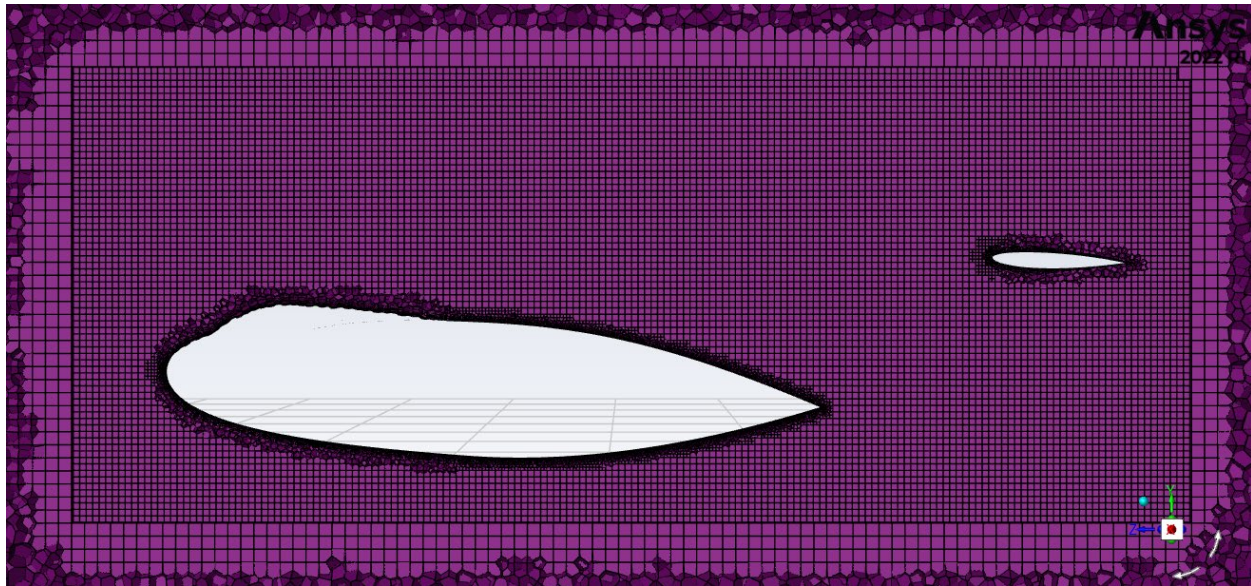


Figure 25: Volume Mesh Around Mid-Section of CBY-3

### 5.1.3 Enclosure Size

The size of the wind tunnel, or enclosure, of the simulations was a key aspect in correctly calculating the aerodynamic properties of the aircraft. When running aerodynamic tests of aircraft in wind tunnels, either physical or simulated, it is important to make sure that the enclosed space is sufficiently large enough to capture all the characteristics of the displaced air without

disturbance, as it would act in normal flight. Based on different sources we consulted, it was recommended to have an enclosure between three and five times the length of the aircraft, as well as more than a wing's length to the side and below [27, 30]. The enclosure size was further determined by personal experimentation and comparing results between different tests.

The enclosures were sized to be 48 feet away from the wingtip and bottom of the aircraft, and five times the aircraft length. For the DC-3, this created an enclosure that was 323 feet and 9 inches long, 95 feet 3 inches wide, and 116 feet tall. For the CBY-3, the enclosure was 270 feet 6 inches long, 90 feet 10 inches wide, and 107 feet 6 inches tall. The lengths of the enclosures were set so that there would be one aircraft length in front of the respective aircraft, and three lengths behind it. For reference, the DC-3 has a total length of 65 feet, and the CBY-3 a length of 54 feet 6 inches. In Figure 22 and Figure 23, the enclosure is the large blue area surrounding all of the components.

In the meshing phase, there was no upper limit specified for the size of the enclosure. By doing this, we would allow the volume mesh of the unlabeled parts of the enclosure (i.e., all of the space outside the second BOI) to be as large as allowable. This further reduced the complexity of the simulation without sacrificing accuracy; This volume of air would have a very negligible effect on the aircraft performance, due to being relatively far away from the aircraft.

#### 5.1.4 Simulation Settings and Physical Models

For each simulation, the model of the aircraft was inserted into the enclosure and the bodies of influence at the simulation's designated angle of attack. For each simulation, the air flow is always parallel to the enclosure prior to interacting with the aircraft. This was done to better simulate the effects of the airflow behind the aircraft, without having to worry about any interactions with the boundaries before the flow stabilized. This did mean, however, that for each test that was run, both the surface and volume mesh had to be recalculated. Although this could have created differences between the meshes for different simulations, since all of the meshes for a given aircraft were generated using the same settings, this difference would be negligible.

As is mentioned in Section 3.3, the turbulence model that was selected for the simulations was the  $k-\omega$  SST model. In the turbulence model, the curvature correction option was also enabled. This helped the turbulence model account for the high curvature at certain points in the aircraft model, such as the leading edges.



Most of the other simulation settings can be found in Section 5.1.1. However, they will be restated here specifically as simulation inputs for clarity. The operating pressure was set to 101325 Pascals, which is standard atmospheric pressure at sea level. The inlet velocity was set to the specified velocity for the aircraft, which was 82.3 meters per second for the CBY-3, and 92.5 meters per second for the DC-3. For both the air inlet and outlet, which were the front and rear face of the enclosure, the turbulent intensity was set to 0.5%, and the turbulent viscosity ratio was set to 2. These values were based on the fact that in wind tunnels, there is usually not much turbulence at these points [30]. This can also be the case for standard, nondisruptive air flows around actual aircraft. The fluid for the simulation was set to air, and the solid surfaces were aluminum.

The tunnel walls, which were the three faces of the enclosure perpendicular to the inlet and outlet that did not touch the aircraft model, were specified as zero shear boundaries. This means that while they did act as boundaries to the air flow, they did not have any boundary layer effect on the airflow. This helped reduce the complexity of the simulation, as it was unnecessary to model these effects. Every other surface in the simulations, namely the aircraft surface, were normal shear surfaces. This meant that boundary layers had to be modeled in the volume mesh, to accurately model the distribution of flow velocity close to the surface.

Additionally, as can be seen in Figure 22 and Figure 23, as well as any depiction of the simulation's model, only half of the aircraft is present. This is due to a feature of Ansys Fluent that allows for a 'symmetry' plane to be specified. This symmetric plane allows for models to be reduced greatly in size, and the calculations done on the half of the model that is present are mirrored for the other side. Although only half of the aircraft is present in the model, the forces calculated account for and include the other mirrored half.

#### 5.1.5 Iterations and Convergence

Each simulation had the maximum number of iterations set to 400. We determined this to be enough for the simulation to either converge or reach a point of steady oscillation. Based on background research, as well as tutorials provided by Ansys, it is not uncommon for complex aerodynamic simulations to reach a point where the residuals do not fully reach convergence and oscillate around a specific value. This can be caused by the turbulent nature of the airflow, which makes it very difficult for the solver to continue to work down the residual values [30]. An example

of this behavior can be seen in Figure 26, where the horizontal axis shows the number of iterations, and the vertical axis shows the value calculated for each residual at the corresponding iteration number. The legend in the top right corner explains which residual is associated with each color line.

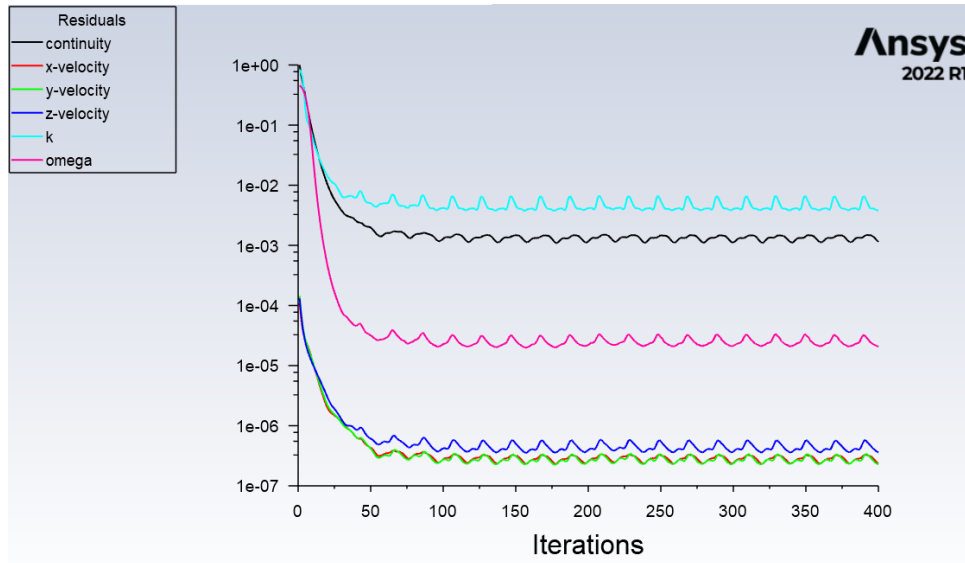


Figure 26: Residual Oscillation and Non-Convergence

Based on the scale of the simulation, which included full size aircraft, we expected that the simulation might have some trouble getting certain values down to the default designation of 0.1% difference. It was also suggested by Dr. Hera that typically the most difficult value to reduce is continuity; also known as the conservation of mass. In order to account for the anticipated discrepancy, we decided to track and note the final value calculated for the difference in mass flow between the inlet and outlet. This would be compared to the total in flow of air into the system, and if it was sufficiently small, the solution would be considered valid.

#### 5.1.6 Data Collection

When Ansys Fluent completes a simulation, it stores a very large variety of data as potential outputs. These outputs can include any of the residuals, static and dynamic pressure, forces, moments, and many others. It was necessary for us to decide what would be used as the source of the data, and how those values would be processed once they were pulled from the completed simulations.

Originally, the data we were planning to evaluate were the coefficients of lift and drag for the overall aircraft, as well as these coefficients for specific parts of the aircraft. However, it was difficult to discern exactly how Ansys Fluent was calculating these coefficient values. It was known, based on some research into the User Guide, that the coefficients were calculated using a user-input reference area. This made it difficult to ensure accurate values were being extracted for the different coefficients, since each one required a different reference area.

To solve this problem, it was decided to instead use the lift and drag force calculated by the simulation, and then calculate the coefficient independently. This way, it was certain that the correct areas were being applied to the correct equations. The equations defining these coefficients can be found in Section 2.3.2.

The reason coefficients we were calculating coefficients instead of just using the lift and drag forces was because of the unitless nature of the coefficients. The coefficient values are calculated by taking the given force and dividing it by the dynamic pressure of the airflow and a reference area the force acts on. By doing this, the coefficient represents a specific property that is not unique to a specific value of airspeed, total area, or air density but rather a nondimensional combination of these parameters. That way, even if two differently sized aircraft were simulated at two different speeds and altitudes, their properties could be accurately compared. This was an important factor of this comparison, since the two aircraft are noticeably different sizes, and are flying at two different airspeeds. This is also convention for all standard aerodynamic analysis, for exactly the same reasons [15, 16, 17].

## 5.2 Results

The data directly collected from the Fluent simulations is available in Appendix C and Appendix D. The lift force and drag forces were converted to coefficients, as described in Section 2.3, and the data was organized and tabulated, as described in Section 3.2. It is important to note that the wing area and aspect ratio for all relevant calculations in Section 2.3 are modified to include the whole area of the aircraft rather than just the area of the wings. This was done to include the fuselage area as part of the total area that produces lift. The approximated values for Oswald efficiency factor are 0.767 and 0.710 for the CBY-3 and the DC-3, respectively. These values are good approximations relative to data provided in the literature [15, 16, 17, 23].

Figure 27 below shows how the lift and drag coefficient changes with angle of attack. As mentioned previously in Section 2.3, the lift coefficient changes linearly with the angle of attack for angles below the stall angle. Therefore, Figure 27 implies that the stall angle for the CBY-3 is greater than  $10^\circ$ . The lift slope for the CBY-3 is 0.0549.

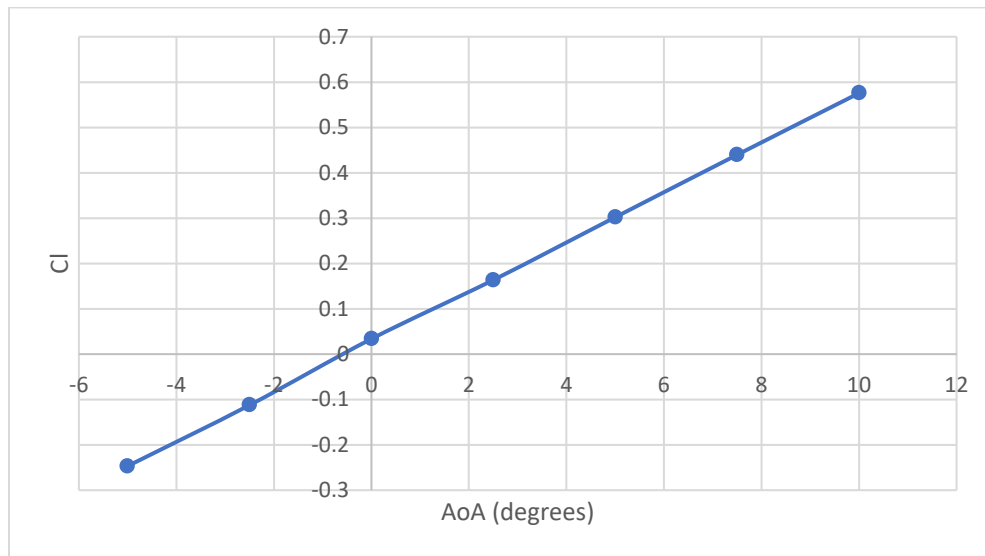


Figure 27: Lift Coefficient v. Angle of Attack – CBY-3

For the Loadmaster, the lift coefficient at low angles of attack was relatively low. At  $0^\circ$  angle of attack, the lift coefficient is very close to 0, which is not unreasonable, but lower than what we originally expected.

Figure 28 below shows how the lift coefficient varies with angle of attack for the DC-3. The lift begins to decrease at around  $8^\circ$ , implying that the plane stalls at an angle of attack of about

8°. However, it is important to keep in mind that the angle of attack for the wings is greater than that of the fuselage by roughly 2.5° (discussed further in section 6.1) so it makes sense that the stall angle would be smaller than expected. Generally, the stall angle for typical aircraft is greater than 10° [17]. The linear portion of the lift slope for the DC-3 is 0.0653.

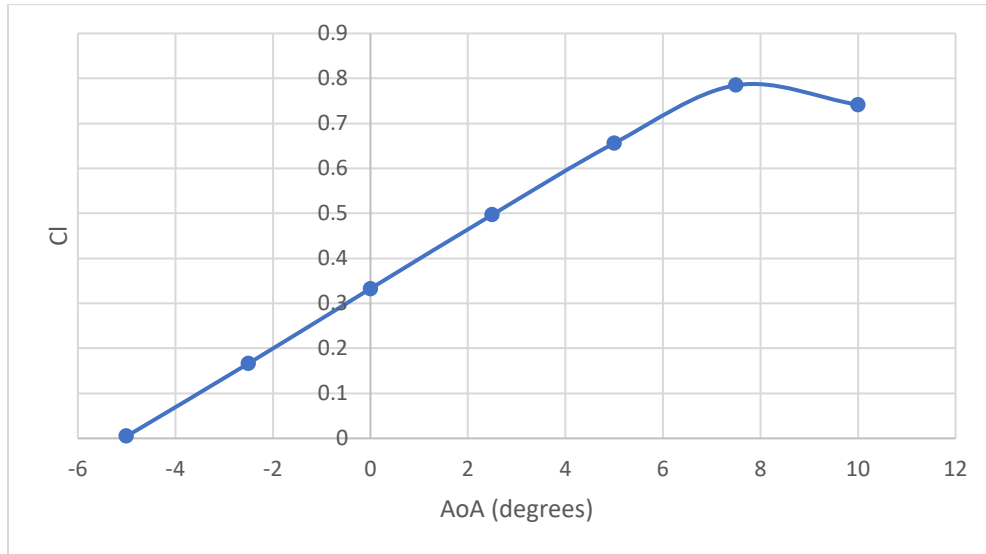


Figure 28: Lift Coefficient v. Angle of Attack – DC-3

Figure 29 below shows the drag polar, or variation of the drag coefficient for different lift coefficient values, of the CBY-3. Generally, the drag is lowest at low angles of attack and increases steeply as the lift increases. The cause of the small increase in drag near zero lift is uncertain, and given more time, we would have investigated it further. Based on the approximated value for the Oswald efficiency factor, the value for the drag coefficient at zero lift, or parasitic drag coefficient for the is 0.0103. This is very close to the estimated value of the y-intercept in Figure 29, which corresponds to the drag coefficient at zero lift for the CBY-3. This implies that both the simulation and the calculated values are close to accurate.

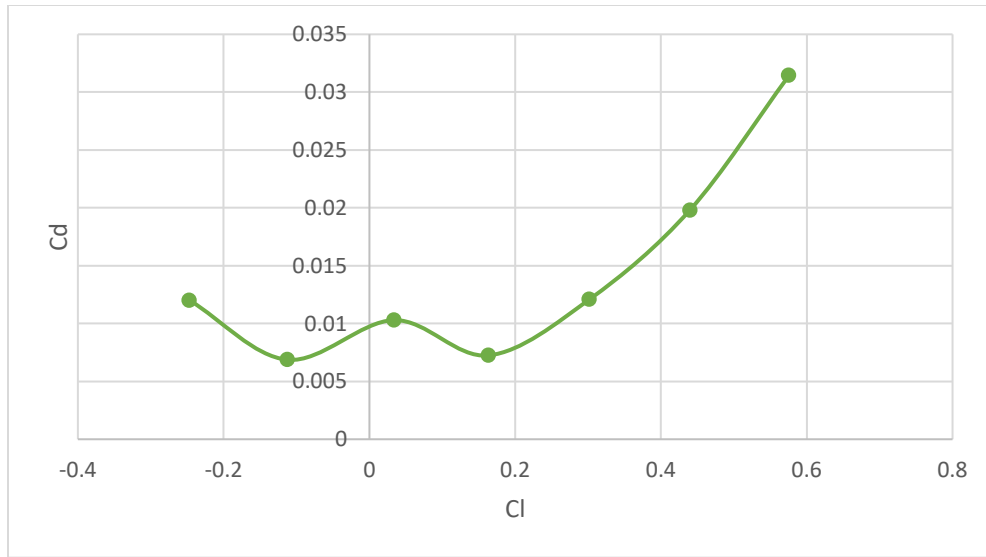


Figure 29: Drag Coefficient v. Lift Coefficient (Drag Polar) – CBY-3

The drag polar for the DC-3 is shown in Figure 30. The curve on the right side of the graph corresponds to the stall angle of attack, hence the drag increases significantly while the lift drops.

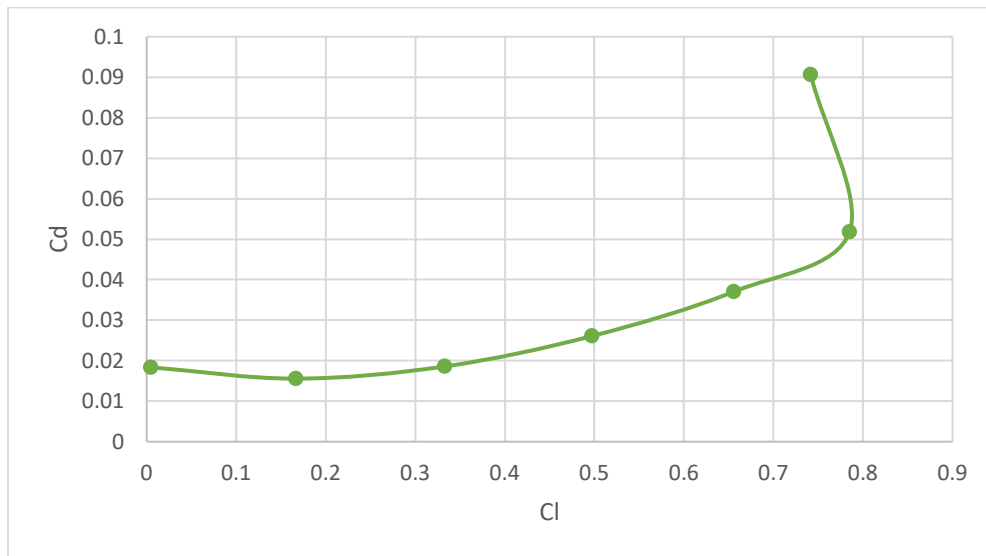


Figure 30: Drag Coefficient v. Lift Coefficient (Drag Polar) - DC-3

Again, the value shown on the graph in Figure 30 is very close to the calculated value for the parasitic drag, which is 0.0144.

Using the Excel calculator described in Section 3.2 and the calculations described in section 2.3, we determined certain performance characteristics summarized in Table 9 below.

Table 9: Calculated Performance Characteristics Summary

Performance Characteristic	CBY-3		DC-3	
	Metric	Imperial	Metric	Imperial
Max L/D	0.0421		0.0467	
Cl at max L/D	0.487		0.616	
Min Drag	398 N	89.5 lbf	360 N	80.9 lbf
Cd at min Drag	0.00122		0.00097	
Airspeed at min Drag	26.2 m/s	58.5 mph	21.1 m/s	47.2 mph
Thrust required	3378 N	759 lbf	5363 N	1206 lbf
Power required	253 kW	339 hp	496 kW	665 hp
Cl at min power	0.844		1.067	
Airspeed at min power	19.9 m/s	44.5 mph	16.0 m/s	35.8 mph

Consistent with Figure 27 and Figure 28, the DC-3 had higher lift coefficients than the CBY-3. Additionally, the maximum lift-to-drag ratio for the DC-3 was higher than that of the CBY-3. Possible reasons for this are explained in further detail in section 6.1. Furthermore, the DC-3 requires less thrust and power to maintain level flight than the CBY-3 and is capable of flying at lower speeds without stalling. This implies that the CBY-3 needs more fuel to maintain steady-level flight than the DC-3, and therefore has a less fuel-efficient design.

We also examined the distribution of pressure across the surface of the two aircraft, as well as on cross-sectional spanwise planes. These pressure contours provided a visual representation of the data we collected. We examined two different pressure contours for each aircraft: the dynamic pressure on the spanwise planes, and the pressure coefficient across the surface of the aircraft. In all of the below figures, the pressure is represented in metric units.

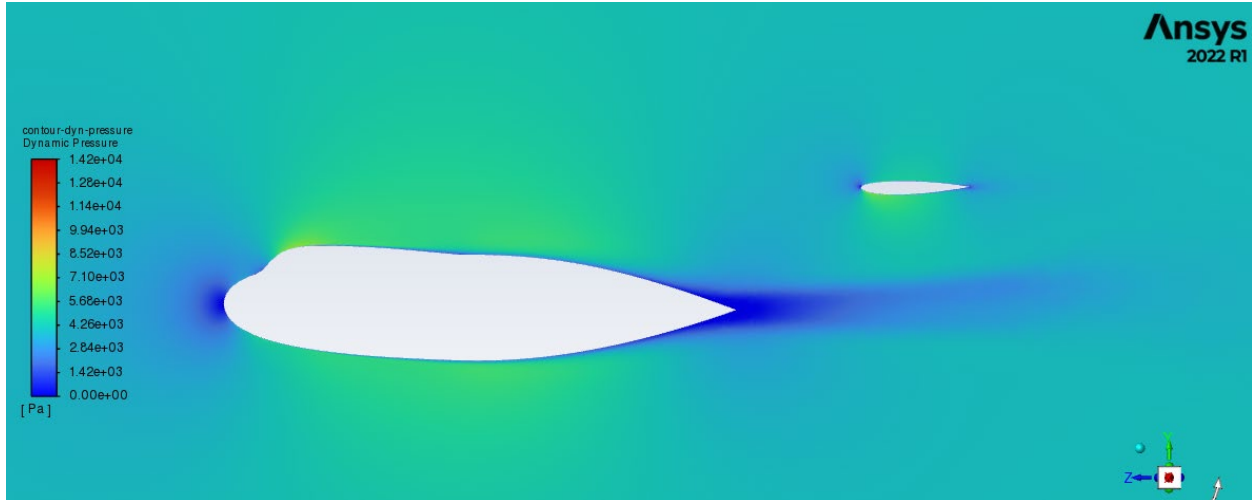


Figure 31: Dynamic Pressure Distribution Around CBY-3 Centerline



Figure 32: Dynamic Pressure Distribution Around DC-3 Centerline

One can see by comparing the difference in pressure distribution around the two fuselages the different lifting characteristics of the two. Although the pressure distribution of the CBY-3 is much more dramatic around the fuselage than in other places of the aircraft, at zero angle of attack, the pressure is relatively evenly distributed between the top and bottom of the fuselage. This helps explain the relatively low lift generated at low angles of attack. One can also see that the ambient dynamic pressure of the surrounding air in the case of the CBY-3 is notably lower than the DC-3, which is due to the lower air flow velocity. A similar observation can be made when comparing the wings of the DC-3 and CBY-3 at the same angle of attack. The below figures display the dynamic pressure distribution around the wings of both aircraft at an angle of attack of 2.5 degrees.



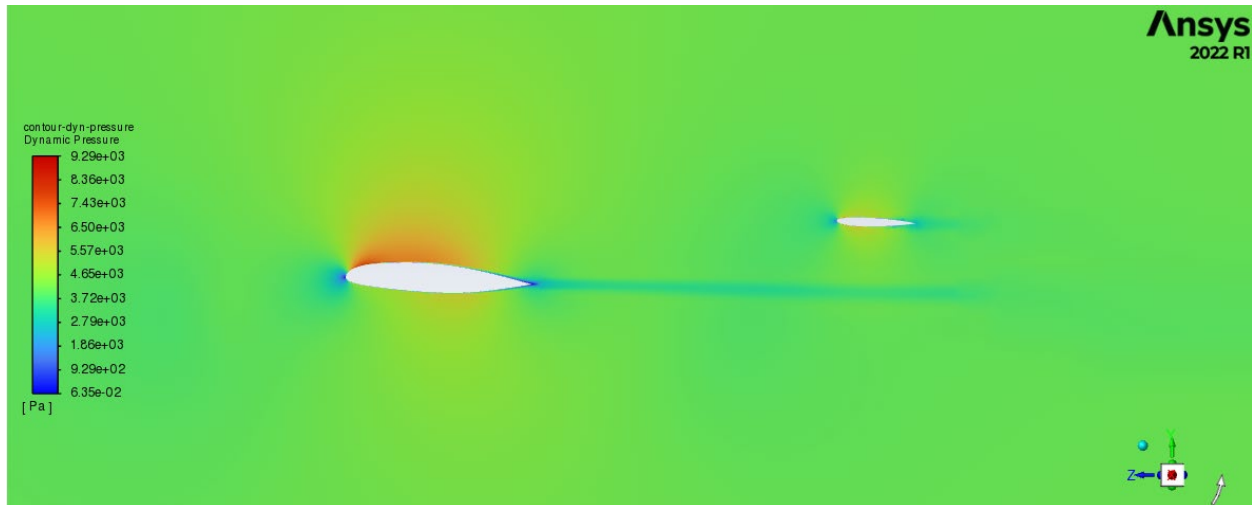


Figure 33: Dynamic Pressure Distribution of CBY-3 Wing, AoA = 2.5°

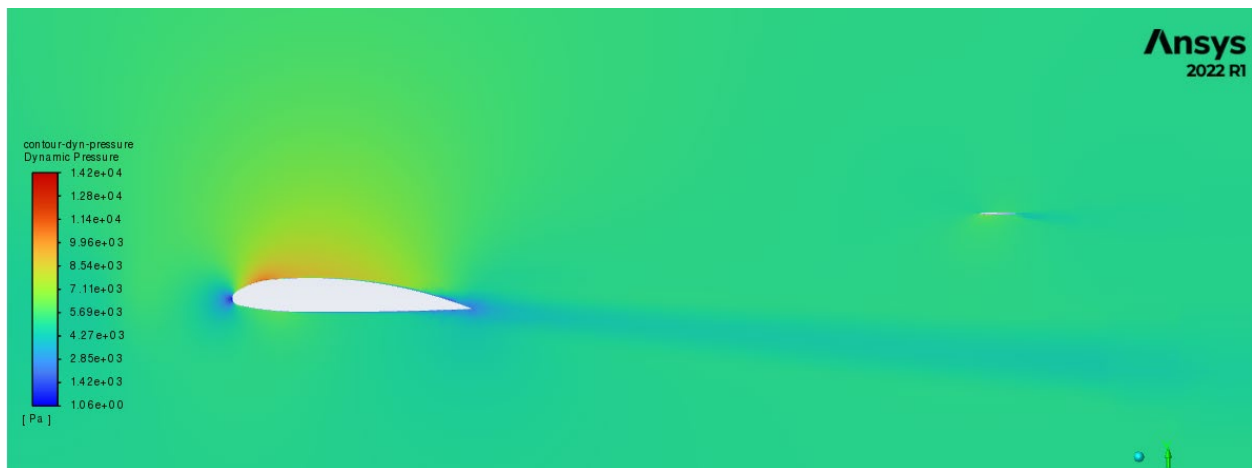


Figure 34: Dynamic Pressure Distribution of DC-3 Wing, AoA = 2.5

One important note when examining the difference in pressure distribution between the two aircraft is the scale displayed. For the CBY-3, the maximum dynamic pressure displayed is about 9,290 pascals, while the DC-3 has a maximum dynamic pressure of 14,200 pascals. This difference in scale was intentional, in order to make the pressure change and distribution more visible. One cause of the difference in pressure is the velocity of the ambient flow, as mentioned in the previous paragraph. By making the scales of the two images relative to the maximum and minimum of the respective system, it is much easier to understand the overall distribution of pressure. The maximum pressures of both wings seem to be concentrated in a small area, while along the rest of the wing the pressure is relatively evenly distributed.

The pressure coefficients of the two aircraft show a similar result, with the wings being relatively similar, and the fuselages being very different. The pressure coefficient, similar to the lift and drag coefficients, is a nondimensional measure of pressure relative to the applied flow. In the same way that the other coefficients are used to compare two different aircraft under different conditions, the pressure coefficients are used to compare the overall pressure on the Loadmaster and the DC-3.

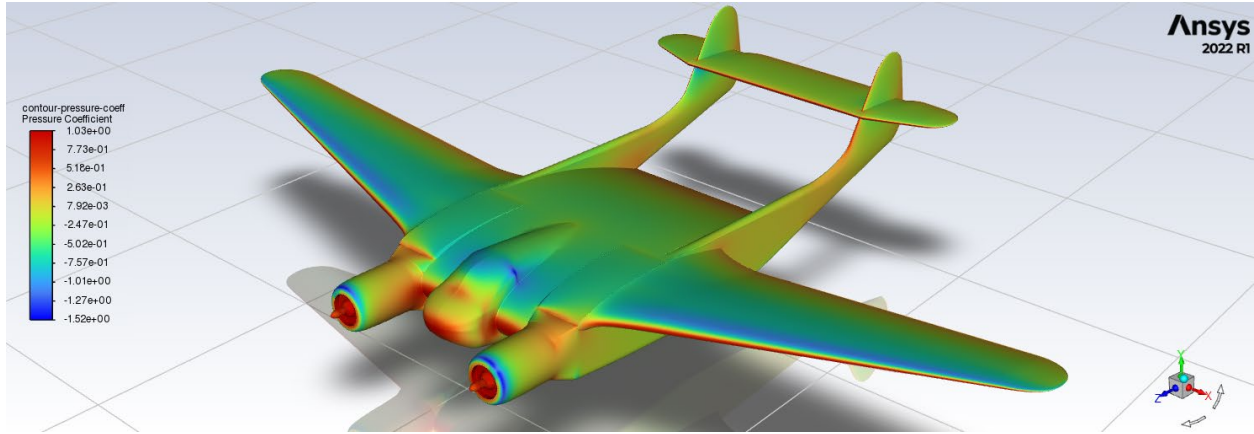


Figure 35: Pressure Coefficient Distribution on CBY-3, AoA = 2.5°

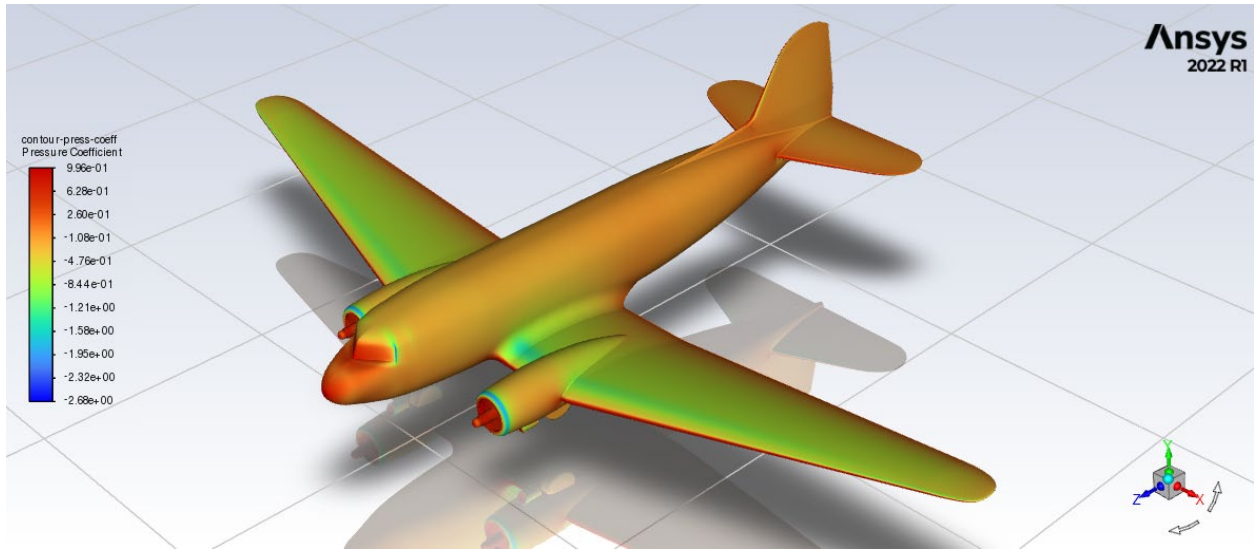


Figure 36: Pressure Coefficient Distribution on DC-3, Wing AoA = 2.5°

The pressure coefficient distribution across the Loadmaster’s fuselage is very similar to the distribution across the tops of the wings, as can be seen in clearly in Figure 35. This distribution is also evident on the DC-3’s wings, however the body of the DC-3 has a very uniform pressure distribution, as shown in Figure 36.

The ranges of pressure coefficient here also help understand the results obtained from the simulation. The CBY-3 and DC-3 both have very close maximums for pressure coefficient, which are 1.03 and 0.996 respectively. However, the DC-3's minimum value is significantly lower, with the minimum pressure coefficient being -2.68. The CBY-3's minimum pressure coefficient is -1.52. Although these extreme values are mostly only found in areas of very sharply varying geometry, it can be seen close to the leading edge of the wing of the DC-3, the pressure is below the minimum value for the Loadmaster.

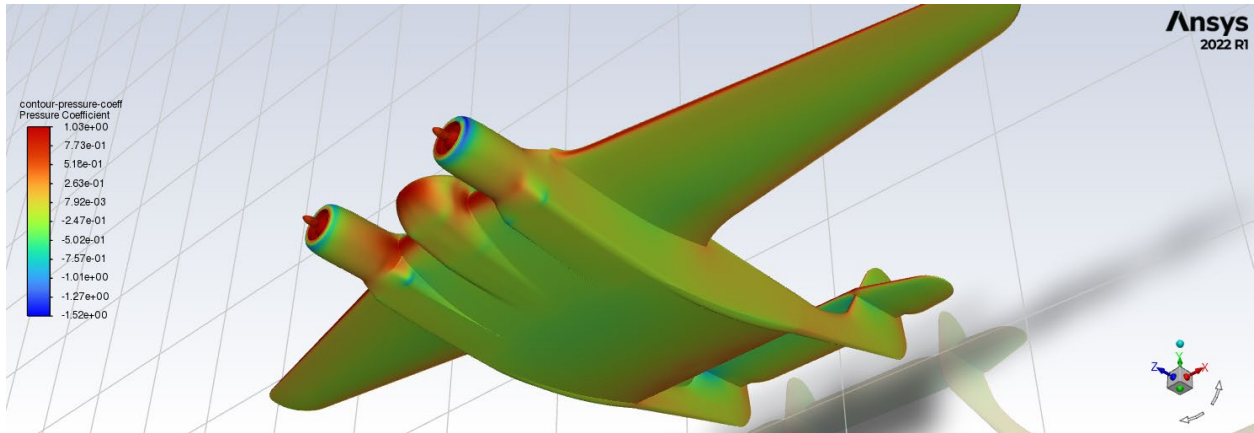


Figure 37: Pressure Coefficient Distribution on Bottom of CBY-3, AoA = 2.5°

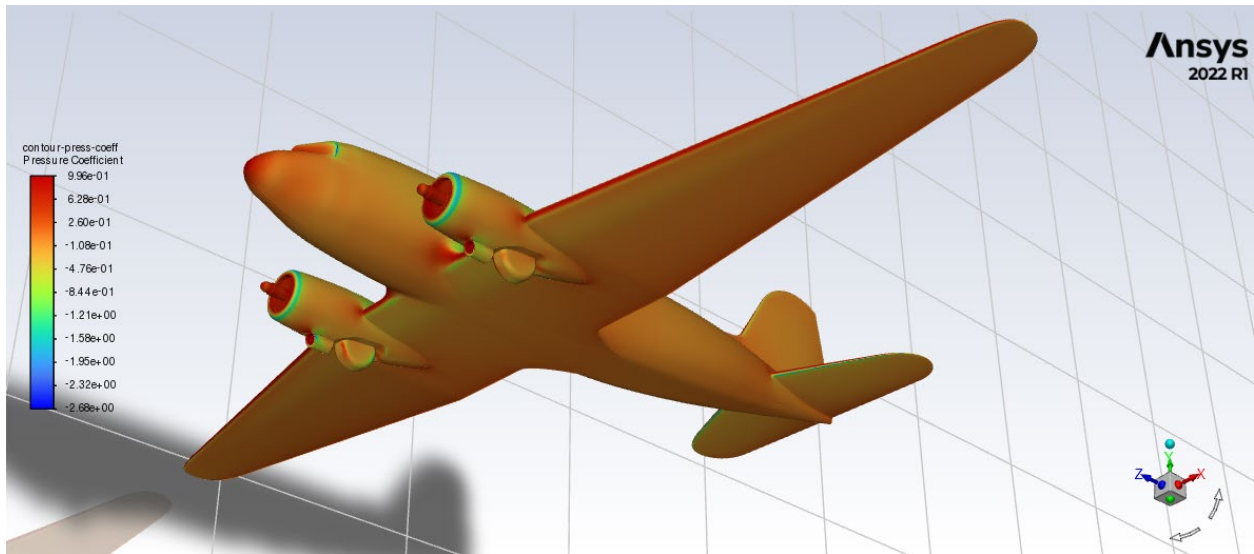


Figure 38: Pressure Coefficient Distribution on Bottom of DC-3, Wing AoA = 2.5°

The bottoms of the two aircraft, shown in Figure 37 and Figure 38 are fairly similar, both having a higher pressure coefficient than is observed on the top of the wings. However, the CBY-

3's pressure coefficient is notably lower than that of the DC-3, which would further contribute to a lower lifting force.

## 6 Conclusions and Recommendations for Future Work

### 6.1 Aircraft Comparisons

Based on the data collected from the simulations, we concluded that the CBY-3 did not have significantly better lifting properties than the DC-3. This is most evident at low angles of attack, where the DC-3 has a clear design advantage. As was stated previously, on the DC-3 the wings are mounted to the body at an angle of approximately 2.5 degrees. This inherent angle of attack allows the DC-3 to fly with the body level, while maintaining a relatively high lift force from the wings. In contrast, the CBY-3's wings were designed to be parallel with the fuselage. Therefore, we expected that at low angles of attack that the Loadmaster would suffer in its total lift force.

Additionally, there is a significant difference between the airfoils of the two aircraft. The DC-3 used a NACA 2215 airfoil [10], which is more cambered than the airfoil of the CBY-3, meaning that the airfoil is more curved or arched. There are many factors that play into the aerodynamics of an airfoil, but generally, a more cambered airfoil provides more lift than a symmetrical one [17]. It is likely that the engineers working on CBY-3 were still refining the exact shape of the airfoil, due to obvious variations between blueprints and drawings of the CBY-3. This can be seen when closely comparing Figure 39 and Figure 40. Also, as mentioned in Section 2.2, there were considerably less drawings and blueprints made for the Loadmaster than usual when constructing an airplane [5]. This underlines the fact that the CBY-3 was still an experimental prototype, and there were still many detail adjustments to be made. It is reasonable to assume that the performance metrics of the CBY-3 would have improved slightly if Burnelli had received the funding to continue working on the Loadmaster.

It was also evident that the DC-3 maintained a superior lifting characteristic at all angles of attack. It is interesting to note that the total vertical force on the DC-3 remained positive even when the aircraft was pitched down by 5 degrees. Although this would mean that the wings are at a true angle of attack of only -2.5 degrees, it was still surprising to see a non-negative result. This result could be cross checked with an airfoil analysis of the DC-3 performed in a program, however

given the time constraints we were not able to perform this check of our results. It should also be noted that the lift coefficient curve starts to resemble behavior characteristic of flow divergence at 10 degrees angle of attack. We do not know whether this is expected to happen at this value of angle of attack, however records on the DC-3 indicate that the expected maximum lift coefficient of the DC-3 is approximately 1.25 [25]. This maximum value of lift coefficient is typically found at or near the angle of attack where flow divergence occurs [15]. Therefore, we originally expected to see the divergent flow behavior at a higher angle of attack.

The inherent angle of attack is also discussed in the Fairchild report on the Loadmaster [26], prepared when the aircraft was first being evaluated. The writers mention that adjusting the design so that the wing would have an angle of attack relative to the body, much like the DC-3, would improve the flight characteristics [26]. They likely made this observation after noting the Loadmaster had to fly at a somewhat nose-high position in order to maintain level flight. This would also explain why the cruising speed of the Loadmaster is notably slower than the DC-3, since the drag increases with angle of attack, as shown in the drag polar in Figure 29.

It should be noted that the fuselage design is not the only difference between the two aircraft, nor is it necessarily the most important. One conclusion that was evident to our team was that the most important difference between the two aircraft was the maturity of their respective designs at the time when the single CBY-3 prototype was completed. The CBY-3, at the times of its testing and final design, was an early prototype that was likely still actively being altered and improved. The addition of the structure on the tail booms, seen in Figure 17, and the lack of them in official documentation, is a perfect example of the still evolving state of the CBY-3. According to the restoration staff at NEAM, the decision to add this structure was made after the plane was built, which is why none of the blueprints include it. The DC-3, on the other hand, was a fully completed design, that had also had multiple different variations made throughout its service life [37].

It should also be noted that, although a smaller aircraft by volume and overall length, the Loadmaster's empty weight was almost 3000 pounds heavier than the DC-3. It is unknown whether this added weight was primarily due to the design of the lifting fuselage, and if so, it raises the question whether the fuselage design was actually a benefit to the aircraft's overall performance.

## 6.2 Loadmaster Lifting Fuselage Properties

The claim that 40% of the lift of the CBY-3 is generated by the lifting fuselage, which is discussed in Section 5.1.1 and Reference 6 is evaluated as a part of our study. The truth of the claim is somewhat reflected in the collected data. The contribution of the fuselage to the total lift was measured from the Fluent simulation in two different ways; one calculation consisted of the ratio of the body lift to the total lift force. The second calculation consisted of the body lift divided by the sum of the wing lift and the body lift. The difference between the two methods was that the latter does not include the vertical force contributed by the horizontal and vertical stabilizers, which tended to be negative. This calculation was made possible by the ability of Ansys Fluent to output the forces generated by specific parts of the model. Based on the way that the model was organized in Fluent, it was very simple to extract this data.

The body lift to total lift ratio was calculated for each angle of attack and had an average of 31.0%. However, there was a notable amount of variation between the different angles of attack. The largest ratio calculated was at 0 angle of attack, which was just under 50.5%. The lowest ratio calculated was approximately 18.8%, which was measured at an angle of attack of -2.5 degrees. Although these two specific cases had a large deviation, the standard deviation of the data collected was 0.1.

The body lift to total lift ratio, without the inclusion of the tail structure, was found to have an average value of 30.4%. Although this value is very close to the first value calculated, this data had much less variation, with the standard deviation of the data being 0.01. However, the largest deviation occurred at the same angles of attack, with the highest (32.5%) at 0 degrees angle of attack, and the lowest (28.5%) corresponding to -2.5 degrees.

Therefore, the lifting fuselage of the Loadmaster in the simulations for this project contributed 30% of the lift of the aircraft. Although this does not match the 40% originally presumed in Reference 6, it is still a very significant amount of the total lift generated by the aircraft.

## 6.3 Recommendations for Future Work

Towards the end of this project, much less time was available to spend on the analysis of the aerodynamic properties than had originally been planned. This was largely due to the time

required to create the model of the Loadmaster, as well as the time required to learn and execute the Fluent simulations. There was also the sudden change in timelines experienced at the beginning of the project, which greatly reduced the time available for the analysis.

Although these studies provide a thoughtful and thorough insight on the aerodynamic properties of the CBY-3 Loadmaster, more tests are required to confirm the data presented here. As well as running tests to confirm the data, it may prove valuable to run tests with a higher mesh fidelity. The time constraint on this project necessitated the use of low mesh densities in order to decrease the simulation time as much as possible.

Furthermore, it would be beneficial to run more accurate and more in-depth calculations based on the data received from the simulations. The calculations done in this study are fundamental equations used for basic aerodynamic analysis and were derived assuming a cylindrical fuselage that provides a negligible amount of lift. This is mainly evident in the wing area,  $S$ , in Equations 2.1 and 2.3, the aspect ratio,  $AR$ , in Equation 2.5, and the Oswald efficiency factor,  $e$ , in Equation 2.6. All these equations were originally designed to only account for the wing area as part of the lifting area [15, 17]. For this study, due to time constraints, we simply added the fuselage area to the wing area, which might not provide the most accurate results. Hence, more thought should be put into correcting these to accurately account for the lifting fuselage.

On top of this, the simulations could be run under many other flight conditions, which could either confirm or deny the results achieved in this project. We chose to only vary the angle of attack, however, performing simulations under combinations of different airspeeds, altitudes, and climbing conditions would be a good way to verify our conclusions.

There is also more depth to aerodynamic analysis of aircraft that was not achieved here. We studied mainly the basic performance characteristics of the aircraft, but metrics like the range, service ceiling, absolute ceiling, and rate of climb can also be calculated. Furthermore, the static and dynamic stability of the aircraft is also valuable to consider. Ansys Fluent is able to provide the moments acting on an aircraft, so a stability analysis of the CBY-3 is certainly possible. We determined that the Loadmaster does not have greater lifting capabilities than the DC-3, but perhaps the fuselage design makes it more stable, which would make it easier to pilot. The stability of the CBY-3 was experimentally measured [26] but could be verified through CFD.

Finally, a shortcoming of the CBY-3 relative to the DC-3 is that the design was not refined and completed, as mentioned in section 6.1. So, to more accurately analyze whether the lifting fuselage concept was more aerodynamically efficient than a cylindrical fuselage, certain design choices of the CBY-3 could be altered to allow a more direct comparison between the plane types. For example, the wing in the model of the CBY-3 could be tilted up slightly to give it an angle of attack of about  $2.5^\circ$  relative to the centerline of the body, similar to the wings on the DC-3. This way, the lift at specific angles of attack could be directly compared without needing to account for the different angles of attack of the wings.

This project can also serve as a sample methodology for similar projects in the future. As there was a limited amount of information and insight on constructing an aircraft from 2D print plans, there were many obstacles we needed to overcome when first starting. We believe that the methodology we generated for creating the solid model of the CBY-3 is a good guideline for future projects.



## 7 References

### 7.1 General References

- [1] New England Air Museum. (2022). *60 Years, 60 Stories*. Retrieved from New England Air Museum: <https://neam.org/pages/60-years-60-stories>
- [2] “Brunelli.” *New England Air Museum*, <https://neam.org/pages/brunelli>. Accessed 12 Oct. 2022.
- [3] Noland , David. “The Burnelli Controversy.” *Smithsonian Magazine* , 1 Nov. 1989, [www.smithsonianmag.com/air-space-magazine/the-burnelli-controversy-15233082/#:~:text=Around%201930%20the%20U.S.%20government,Burnelli%20refused.](http://www.smithsonianmag.com/air-space-magazine/the-burnelli-controversy-15233082/#:~:text=Around%201930%20the%20U.S.%20government,Burnelli%20refused.)
- [4] Wood, Richard. The Contributions of Vincent Justus Burnelli - NASA Technical Reports Server (NTRS). 1 Jan. 2003, [ntrs.nasa.gov/citations/20030004233](https://ntrs.nasa.gov/citations/20030004233).
- [5] Conrath, R. (2004). From Railway Boxcars to a Flying Boxcar. *CAHS Journal*.
- [6] Pelzer, J. D. (1997). Burnelli and His Flying Fuselage. *Aviation History Magazine*.
- [7] Bardehle, Peter. (1985). *THE DC-3 STORY – A Plane that Changed the World*. Retrieved from <https://www.youtube.com/watch?v=bkXHx0i2vHs>
- [8] *Douglas DC-3 | National Air and Space Museum*. [https://airandspace.si.edu/collection-objects/douglas-dc-3/nasm\\_A19530075000](https://airandspace.si.edu/collection-objects/douglas-dc-3/nasm_A19530075000). Accessed 3 Dec. 2022.
- [9] Holden, Henry M., and Henry M. Holden. “DC-3 Specifications.” *Douglas DC-3/Dakota History*, 8 Nov. 2013, <http://www.dc3dakotahistory.org/specs-stats/dc-3-specifications/>.
- [10] Assadourian, A. & Harper, J.A. (1953). Technical Note 3088: Determination of the Flying Qualities of the Douglas DC-3 Airplane. NACA
- [11] Kellari, Demetrios, et al. “Architectural Decisions in Commercial Aircraft from the DC-3 to the 787.” *Journal of Aircraft*, vol. 55, no. 2, 2018, pp. 792–804, <https://doi.org/10.2514/1.C034130>.
- [12] Dorr, R. F. & Borch, F. L. (2008) C-47 carried out duties from WWII until 1970s. *Air Force Times*. 36–. <https://infoweb-newsbank-com.ezpv7-web-p->

[u01.wpi.edu/apps/news/document-view?p=AWNB&t=pubname%3AAFTB%21Air%2BForce%2BTimes&sort=YMD\\_date%3AD&fld-base-0=alltext&maxresults=20&val-base-0=c-47%20carried%20out%20duties%20from%20WWII%20until%201970s&docref=news/11E32B245CAA9B98](http://u01.wpi.edu/apps/news/document-view?p=AWNB&t=pubname%3AAFTB%21Air%2BForce%2BTimes&sort=YMD_date%3AD&fld-base-0=alltext&maxresults=20&val-base-0=c-47%20carried%20out%20duties%20from%20WWII%20until%201970s&docref=news/11E32B245CAA9B98)

- [13] National Air and Space Museum. (n.d.). *Pratt & Whitney Twin Wasp R-2000 (2SD13-G), 2-Row, Radial Engine*. Retrieved from National Air and Space Museum: [https://airandspace.si.edu/collection-objects/pratt--whitney-twin-wasp-r-2000-2sd13-g-2-row-radial-engine/nasm\\_A19560050000](https://airandspace.si.edu/collection-objects/pratt--whitney-twin-wasp-r-2000-2sd13-g-2-row-radial-engine/nasm_A19560050000)
- [14] National Air and Space Museum. (n.d.). *Pratt & Whitney Twin Wasp R-1830-90C (R-1830-S3C4-G), 2-Row, Radial 14 Engine*. Retrieved from National Air and Space Museum: [https://airandspace.si.edu/collection-objects/pratt--whitney-twin-wasp-r-1830-90c-r-1830-s3c4-g-2-row-radial-14-engine/nasm\\_A19600115000](https://airandspace.si.edu/collection-objects/pratt--whitney-twin-wasp-r-1830-90c-r-1830-s3c4-g-2-row-radial-14-engine/nasm_A19600115000)
- [15] Napolitano, M. R. (2012). *Aircraft Dynamics: From Modeling to Simulation*. Hoboken: John Wiley & Sons, Inc.
- [16] Raymer, D. P. (2018). *Aircraft Design: A Conceptual Approach*. American Institute of Aeronautics and Astronautics.
- [17] Anderson, J. D. (2017). *Fundamentals of Aerodynamics*. New York: McGraw-Hill Education.
- [18] Kundu, P. K. & Cohen, I. M. (2008). *Fluid Mechanics*. Burlington: Academic Press.
- [19] Sutthison, D., Wongkamchang, P. & Sukuprakarn, N. 2022, "Aerodynamic Studies of Small Box-Wing Unmanned Aerial Vehicle Using CFD", *Journal of Physics: Conference Series*, vol. 2235, no. 1, pp. 012070.
- [20] Manikantissar & Geete A. 2017, "CFD Analysis of conceptual Aircraft body", *International Research Journal of Engineering and Technology*, 4 217-22
- [21] Shanthamraju Rajiv Rao , Sarla Srinath , Vajrala Bhargavi, Bharathraj Reddy Dere, 2014, Analysis of Vertical Take – off & Landing Aircraft using CFD, INTERNATIONAL JOURNAL OF ENGINEERING RESEARCH & TECHNOLOGY (IJERT) Volume 03, Issue 09 (September 2014), <https://www.ijert.org/analysis-of-vertical-take-off-landing-aircraft-using-cfd>

- [22] Schindler, K., Reckzeh, D., & Scholz, U. (2010). Aerodynamic Design of High-Lift Devices for Civil Transport Aircraft Using RANS CFD. *American Institute of Aeronautics and Astronautics Applied Aerodynamics Conference*.
- [23] Niță, M., & Scholz, D. (2012). Estimating The Oswald Efficiency Factor From Basic Aircraft Geometrical Parameters. *Aero - Aircraft Design and Systems Group*.
- [24] CREAFORM. (2022). *HandySCAN 3D | SILVER Series*. Retrieved from CREAFORM: <https://www.creaform3d.com/en/handyscan-3d-silver-series-professional-3d>
- [25] Quebecair Inc. Regulations. (1957, January 10). Performance Information. *The DC-3 Manual*. Quebecair Inc.
- [26] Fairchild Aircraft Division of Fairchild Engine & Airplane Corporation. (1953). *Evaluation of the Burnelli CBY-3 Transport Design*. Hagerstown Maryland: Fairchild Stratos Corporation.
- [27] Pereira, R. L. (2010). *Validation of software for the calculation of aerodynamic coefficients with a focus on the software package Tornado*. Linköping University.
- [28] Sack, J.-R., & Urrutia, J. (Eds.). (2000). *Handbook of Computational Geometry*. Elsevier B.V. doi:<https://doi.org/10.1016/B978-0-444-82537-7.X5000-1>
- [29] ANSYS FLUENT. (2010). *ANSYS FLUENT Documentation*. Retrieved from ANSYS: <https://www.afs.enea.it/project/neptunius/docs/fluent/index.htm>
- [30] ANSYS FLUENT. (2022). *Aerodynamics of an FSAE Car*. Retrieved from Ansys Innovation Space: <https://courses.ansys.com/index.php/courses/aerodynamics-of-an-fsae-car/>
- [31] From John A.C. Kentfield, Aircraft with outboard horizontal stabilizers, history, current status, development potential, *Progress in Aerospace Sciences*, Volume 45, Issues 6–8, 2009, Pages 169-202, ISSN 0376-0421, <https://doi.org/10.1016/j.paerosci.2009.07.001>.
- [32] Man, M. (2021, November 28). The Douglas DC-3 - Solidworks 2020. Retrieved from <https://grabcad.com/library/the-douglas-dc-3-solidworks-2020-1>

- [33] GrabCAD. (2017). *About GrabCAD*. Retrieved from GrabCAD:  
<https://resources.grabcad.com/company/>
- [34] Massari, A., Boyer, A., Moore, J., Paszczuk, N., Raynowska, E., and Tims, G. “Structural Design Analysis of the Burnelli CBY-3 Loadmaster” WPI Major Qualifying Project (MQP) Report No. 30931, Advisor: J. Blandino, 2023
- [35] Microsoft. (2022). *Basic tasks in Excel*. Retrieved from Microsoft:  
<https://support.microsoft.com/en-us/office/basic-tasks-in-excel-dc775dd1-fa52-430f-9c3c-d998d1735fca>
- [36] Dassault Systèmes . (2022). *We are the 3DEXPERIENCE Company*. Retrieved from 3DS: [https://www.3ds.com/about-3ds?\\_gl=1\\*1juxvuu\\*\\_ga\\*MzMyMDYxMjk1LjE2NzE1NjAyMzY.\\*\\_ga\\_XQJPQWHZH\\*MTY3MTU2MjkwMy4yLjEuMTY3MTU2Mjk0My4yMC4wLjA](https://www.3ds.com/about-3ds?_gl=1*1juxvuu*_ga*MzMyMDYxMjk1LjE2NzE1NjAyMzY.*_ga_XQJPQWHZH*MTY3MTU2MjkwMy4yLjEuMTY3MTU2Mjk0My4yMC4wLjA)
- [37] Gradidge, J. M. (2006). *The Douglas DC-1/DC-2/DC-3: The First Seventy Years*. Tonbridge, Kent: Air-Britain Historians.
- [38] Henderson, D. P. (2022). *THE 8 DECADE HISTORY OF DC-3 N28AA*. Retrieved from Sunshine Skies: <https://www.sunshineskies.com/n28aa.html>

## 7.2 NEAM Archive Sources

The references listed in Table 10 are part of the extensive archive of original sources related to the CBY-3 Loadmaster maintained by the New England Air Museum. The table lists the sources referenced throughout this report and includes the document box number as well as the document name and identification number. Partial or complete images of these documents are available in Appendix A.

Table 10: NEAM Archive Sources

Reference Number	Box Number	Document Name
[NA1]		Loadmaster II, Cargo Version Patent File
[NA2]	B-6A	Basic Dimensions of Wing & Spars Sketch № 23
[NA3]	B-6A	Descriptive View of Spar Flanges Sketch № 21
[NA4]	B-6B	G.A Tail Unit 3-2000A
[NA5]	B-1B	Layout – Fuselage Side Panel P-30002
[NA6]	B-2A	Datum Points SK-3.125
[NA7]	B-2A	Body Master Layout L3-0201

## 8 Appendices

### Appendix A: Pictures and Description of Original Loadmaster Design Documents Used

Table 11: NEAM Archive Documents Use

Reference Number	Document Name	Description/Application
[NA1]	Loadmaster II, Cargo Version Patent File	Layout, outline, and essential dimensions of most recent design version of the Loadmaster
[NA2]	Basic Dimensions of Wing & Spars Sketch № 23	Dimensions of wing airfoil, leading edge camber, dihedral angle, wing heights
[NA3]	Descriptive View of Spar Flanges Sketch № 21	General dimensions of wing
[NA4]	G.A Tail Unit 3-2000A	1/8 scale drawing of tail boom, horizontal stab., vertical stab. Lengths and curvatures dimensioned
[NA5]	Layout – Fuselage Side Panel P-30002	Side profile of fuselage airfoil and details
[NA6]	Datum Points SK-3.125	Specific dimensions of key points on assembled aircraft
[NA7]	Body Master Layout L3-0201	Dimensions and profile view of fuselage, attachment point of tail booms, engine cowls, other features

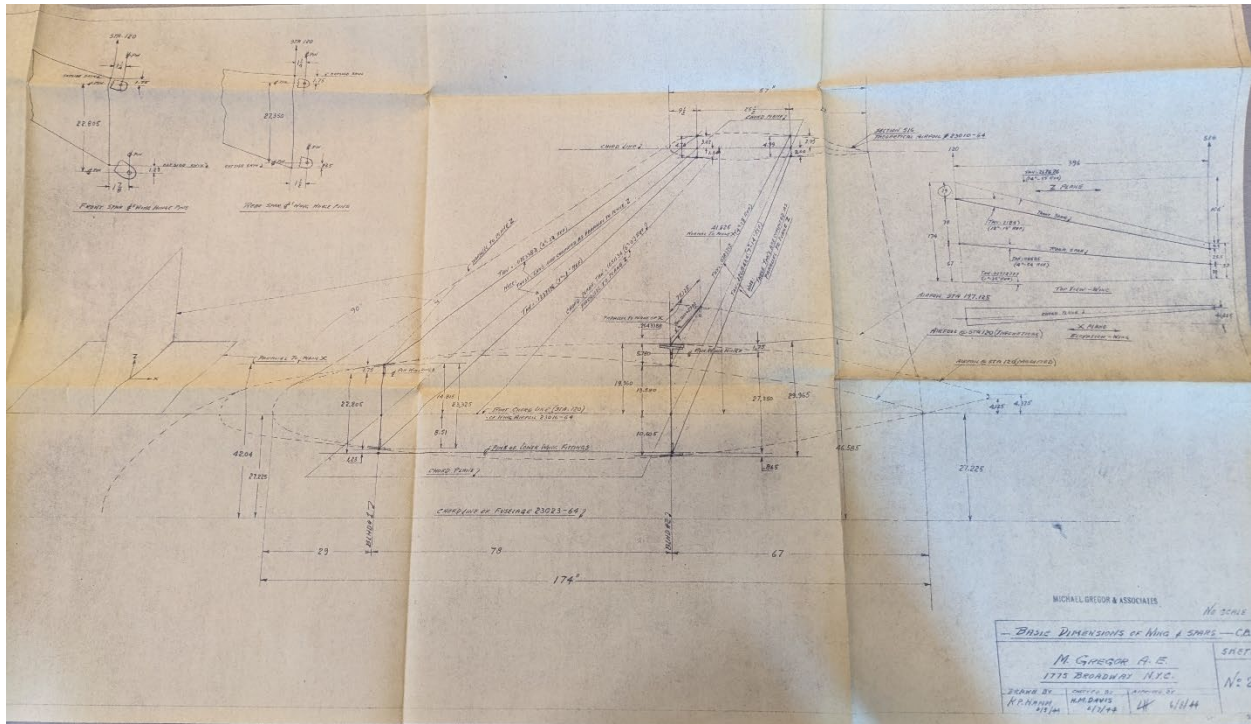


Figure 39: Basic Dimensions of Wing & Spars [NA2]

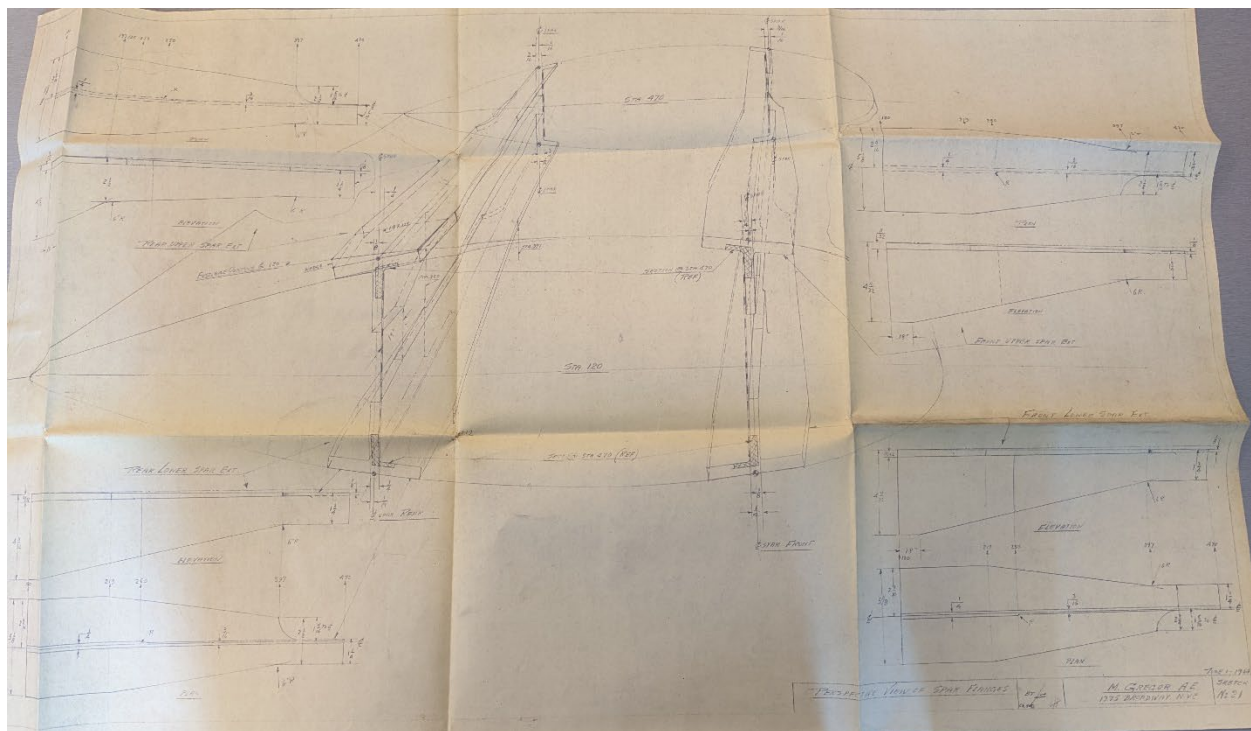


Figure 40: Descriptive View of Spar Flanges [NA3]



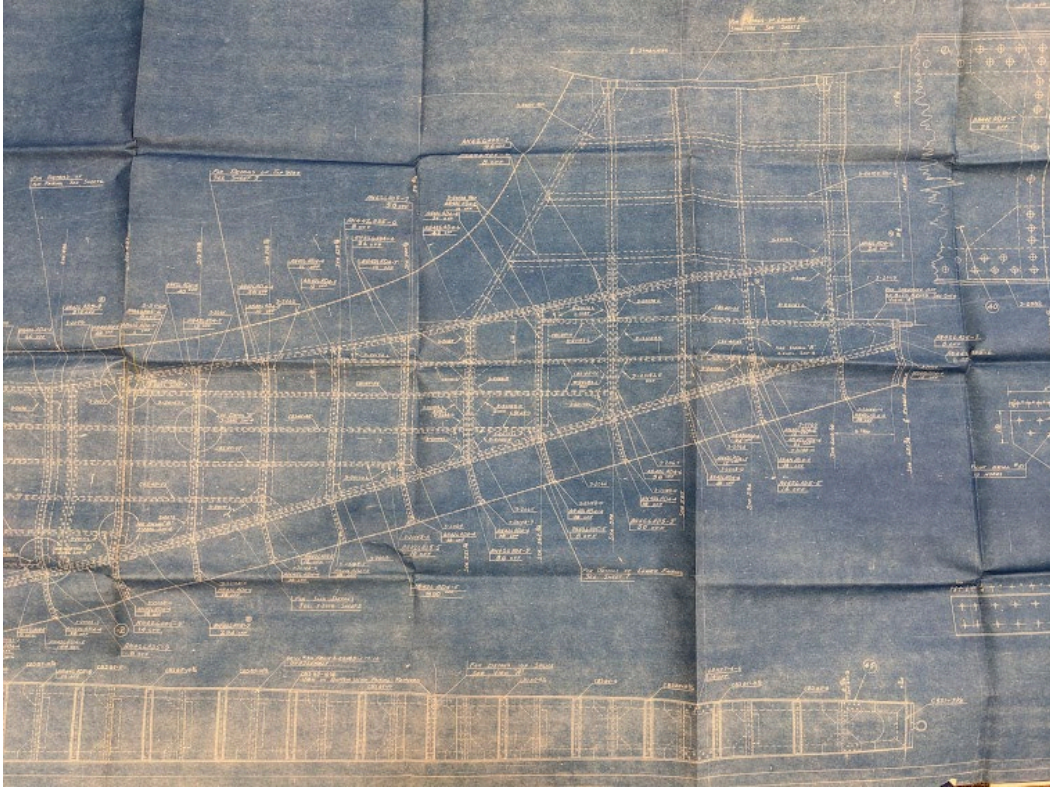


Figure 41: General Assembly: Tail Unit - Vertical Stabilizer [NA4]



Figure 42: General Assembly: Tail Unit: Both Stabilizers [NA4]



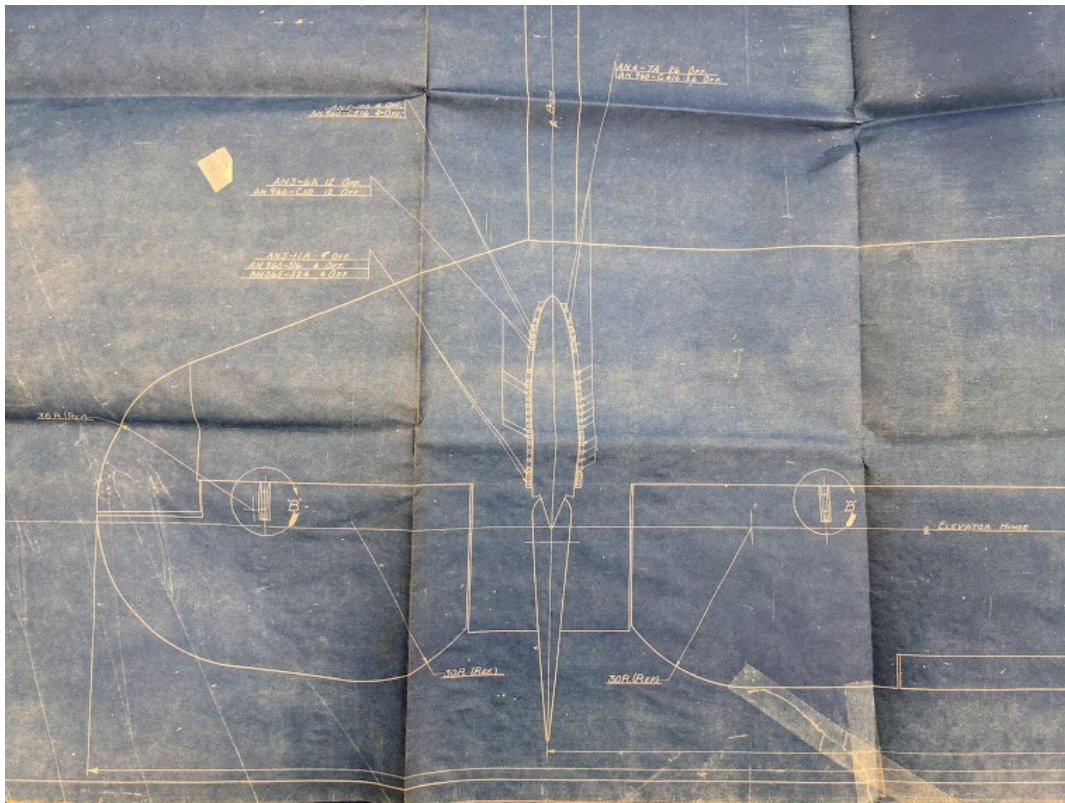


Figure 43: General Assembly: Tail Unit: Horizontal Stabilizer [NA4]



Figure 44: Body Layout: Stitched Together from Multiple Pictures [NA5]



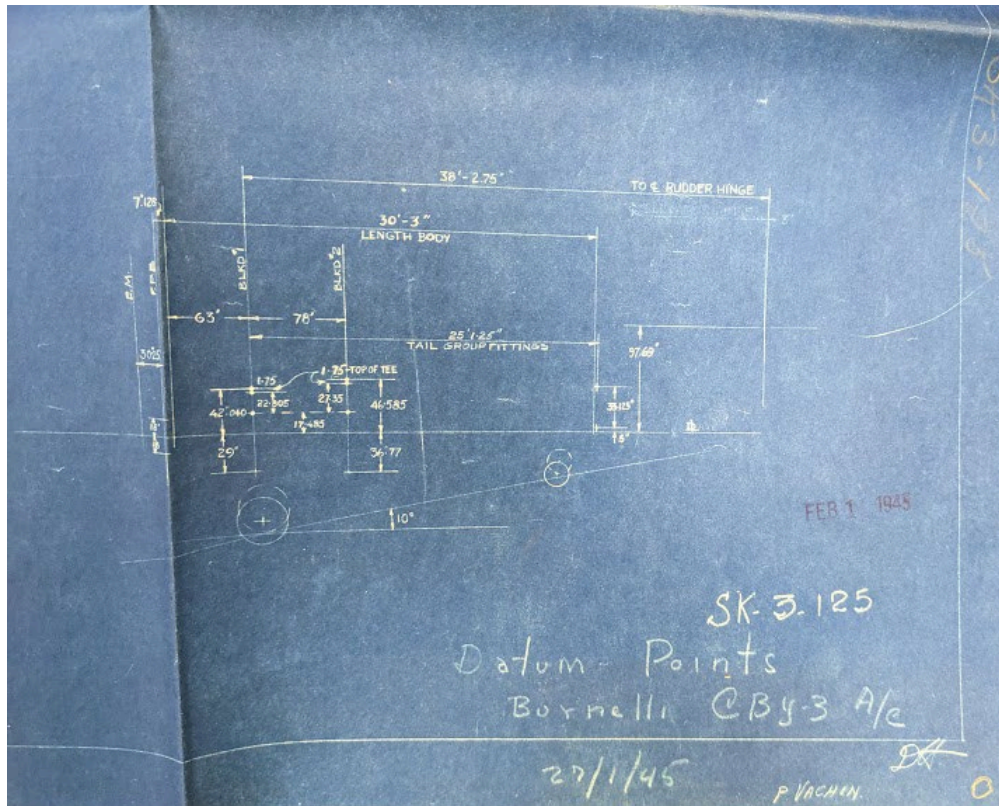


Figure 45: Datum Points - Side View [NA6]

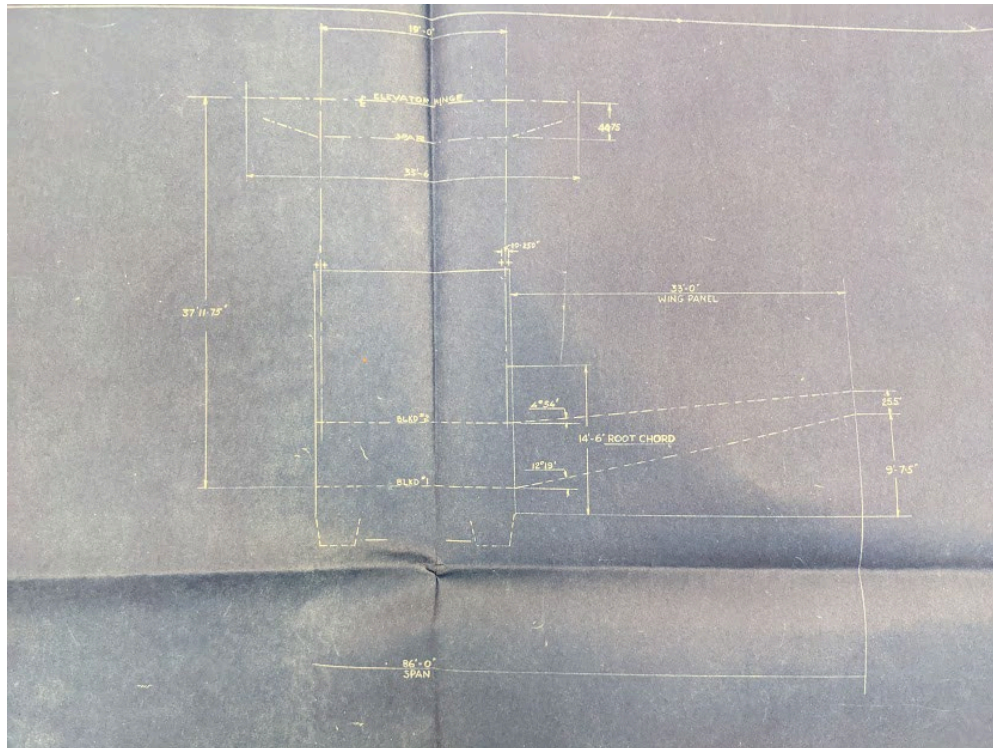


Figure 46: Datum Points - Top View [NA6]

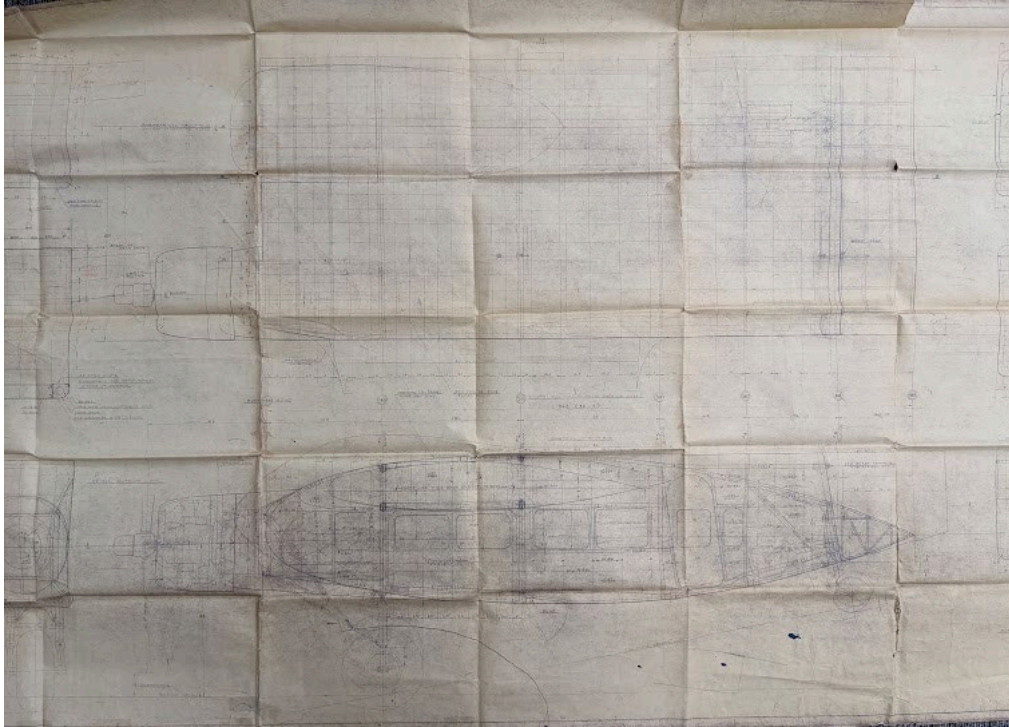


Figure 47: Body Master Layout - Side and Top [NA7]

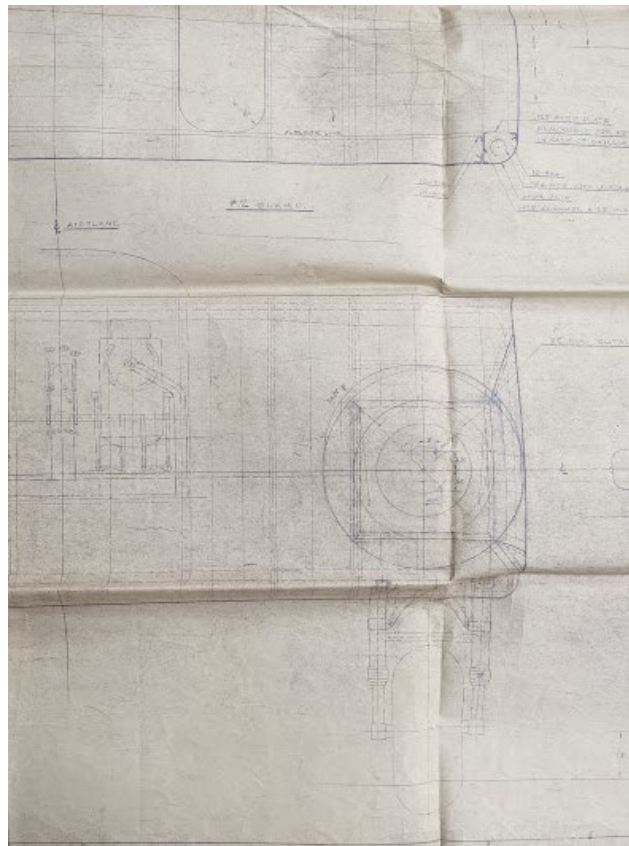


Figure 48: Body Master Layout - Front [NA7]



Appendix B: Loadmaster Key Dimensions

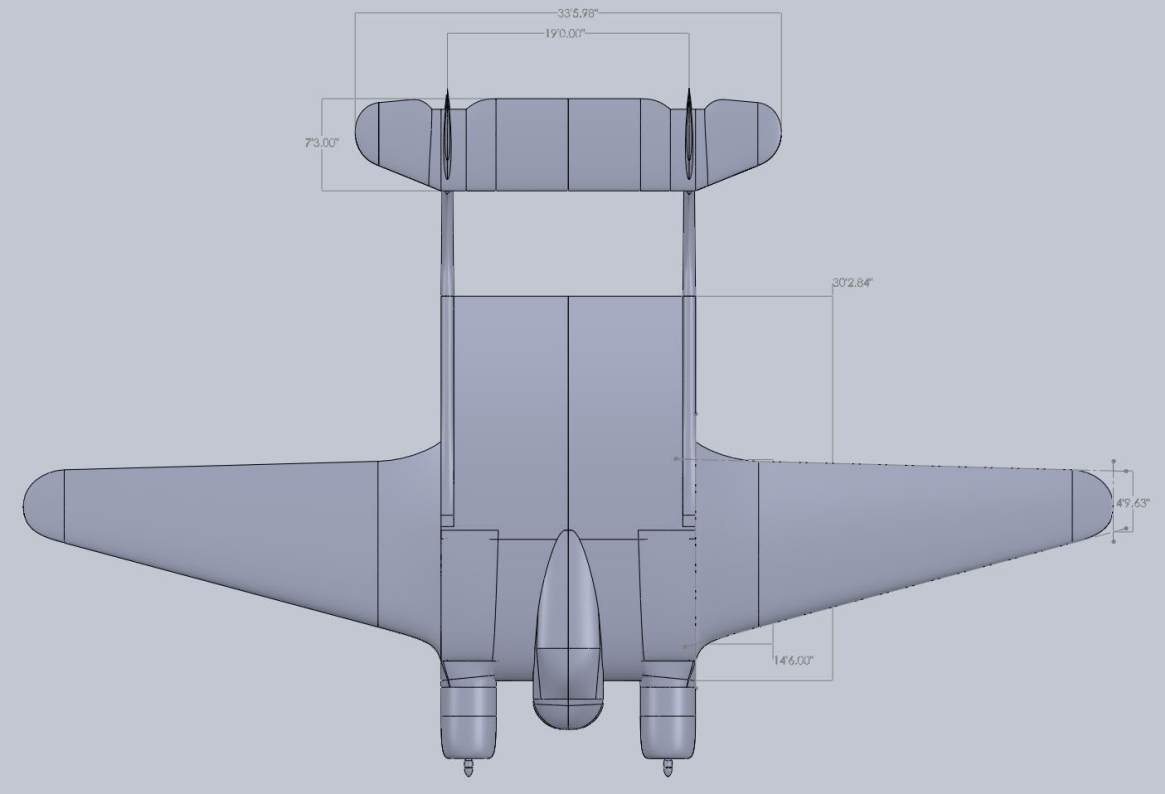


Figure 49: Loadmaster Dimensions - Top View

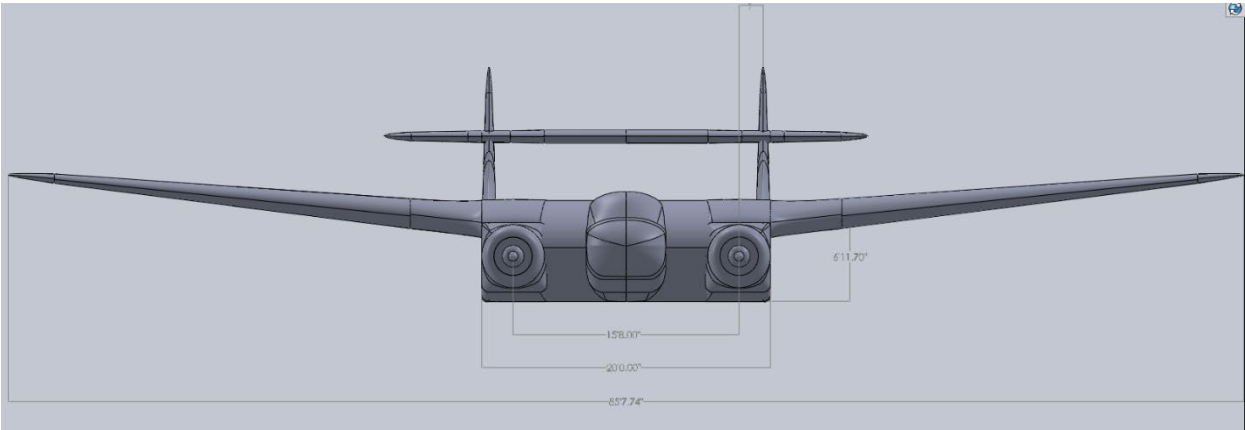


Figure 50: Loadmaster Dimensions - Front View

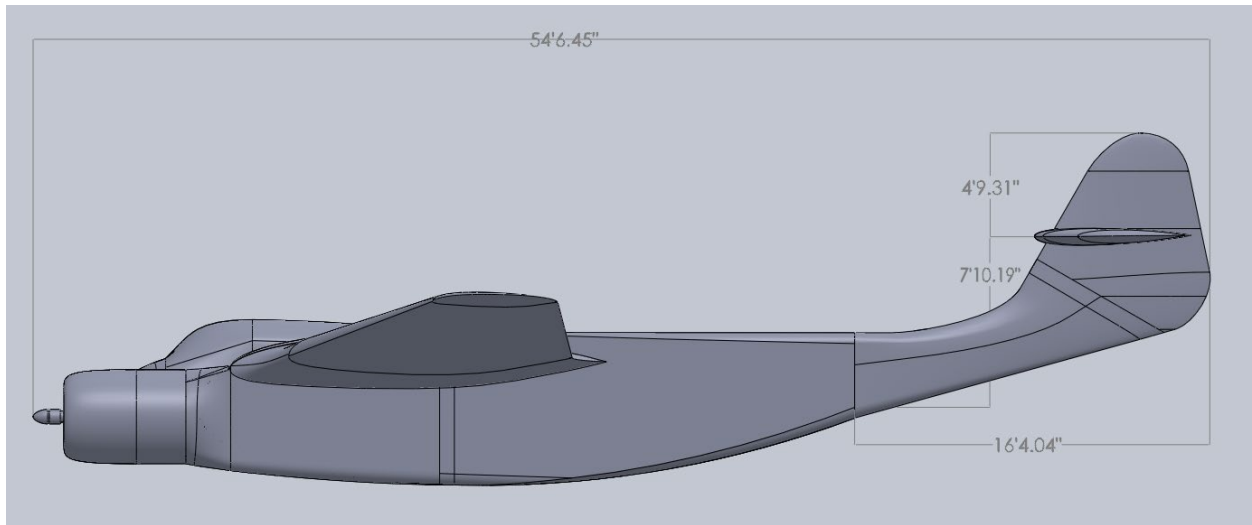


Figure 51: Loadmaster Dimensions - Right View

## Appendix C: Loadmaster Ansys Fluent Data

Table 12: Data Collected from Ansys Fluent for Loadmaster

<b>CBY-3</b>											
Sim	Angle of Attack	Total Lift (N)	Total Lift (lbf)	Total Drag (N)	Total Drag (lbf)	Wing Lift (N)	Wing Lift (lbf)	Body Lift (N)	Body Lift (lbf)	mdot difference (kg/s)	Convergence?
x3-1	0	10987.5	2470.2	3356.2	754.5	11519.4	2589.8	5553.1	1248.4	0.00272	n
x5-2	5	98430.3	22129.1	3942.8	886.4	69410.7	15604.9	30110.0	6769.3	0.00256	n
x5-3	10	187654.6	42188.5	10249.7	2304.3	127157.7	28587.6	55369.4	12448.2	0.00083	n
x5-4	-5	-80460.0	-18089.0	3915.4	880.3	-45252.9	-10173.8	-18574.9	-4176.0	0.00522	n
x5-5	-2.5	-36651.1	-8239.9	2240.4	503.7	-17222.7	-3872.0	-6876.4	-1546.0	0.00001	y
x5-6	2.5	53314.3	11986.1	2363.5	531.4	40510.3	9107.5	18566.0	4174.0	0.00304	y
x5-7	7.5	143324.0	32222.1	6456.6	1451.6	98367.4	22115.0	42698.4	9599.5	0.00375	y

## Appendix D: DC-3 Ansys Fluent Data

Table 13: Data Collected from Ansys Fluent for DC-3

<b>DC-3</b>											
Sim	Angle of Attack	Total Lift (N)	Total Lift (lbf)	Total Drag (N)	Total Drag (lbf)	Wing Lift (N)	Wing Lift (lbf)	Body Lift (N)	Body Lift (lbf)	mdot difference (kg/s)	Convergence?
x5-1	0	123642.1	27797.2	6902.5	1551.8	110885.8	24929.4	15563.9	3499.1	0.0011	n
x5-2	5	243782.0	54807.1	13778.9	3097.8	212030.9	47668.8	26346.7	5923.3	0.0097	n
x5-3	10	275554.0	61950.1	33689.2	7574.0	229631.0	51625.7	23548.0	5294.1	0.0610	n
x5-4	-5	1763.9	396.6	6822.9	1533.9	9016.8	2027.2	4096.2	920.9	0.0005	y
x5-5	-2.5	61910.5	13918.7	5787.0	1301.0	59076.7	13281.6	9841.3	2212.5	0.0019	y
x5-6	2.5	184761.5	41538.1	9692.7	2179.1	162401.0	36511.0	21085.3	4740.4	0.0066	n
x5-7	7.5	291656.2	65570.2	19236.3	4324.7	251489.1	56539.8	29483.9	6628.6	0.0049	n

# Appendix E: Team Gantt Chart and Organization of Tasks

TASK	ASSIGNED TO	PROGRESS	START	END
<b>Goal 1</b>				
<b>Objective 1</b>				
1. Research the history of the CBY-3 and DC-3	Whole Team	100%	8/24/22	10/13/22
3. Research and identify key technical performance metrics for the CBY-3, e.g. payload, range, max altitude, max speed, required take-off distance, etc.	Maria, Aaron, Gabi, Nick P	100%	8/24/22	11/11/22
5. Review and identify any published work describing CFD analysis of entire aircraft; what parameters are evaluated using CFD, e.g. lift, drag, stall characteristics, etc.	Maria, Nick O	100%	10/25/22	11/4/22
6. Research and identify how to set up Fluent simulation domain, including correct boundary conditions	Maria, Nick O	100%	10/25/22	11/4/22
8. Prepare table of cases (i.e. "test matrix") to be evaluated in Fluent for each aircraft	Maria, Nick O	100%	11/4/22	11/16/22
9. Import CBY-3 solid model into Fluent	Maria, Nick O	100%	11/16/22	11/20/22
10. Import DC-3 solid model into Fluent	Maria, Nick O, Nick P	100%	10/25/22	11/20/22
11. Perform Fluent simulation of CBY-3, including post-processing	Maria, Nick O	100%	11/20/22	12/8/22
12. Perform Fluent simulation of DC-3, including post-processing	Maria, Nick O	100%	11/20/22	12/8/22
13. NEAM Visit 1	Whole Team	100%	9/21/22	9/21/22
14. NEAM Visit 2	Maria, Nick O, Amaya, Emily, Gabi, Nick P.	100%	11/10/22	11/10/22
<b>Objective 2</b>				
1. Research and identify methodology (steps) to create solid (CAD) model from 2D plan	Maria, Nick O, Aaron	100%	8/24/22	10/13/22
6. Construct at least one solid model of the CBY-3 constructed from 2D plans	Maria, Nick O	100%	8/24/22	11/11/22
7. Construct at least one solid model of the DC-3 constructed from 2D plans	Whole Team	100%	8/31/22	8/31/22

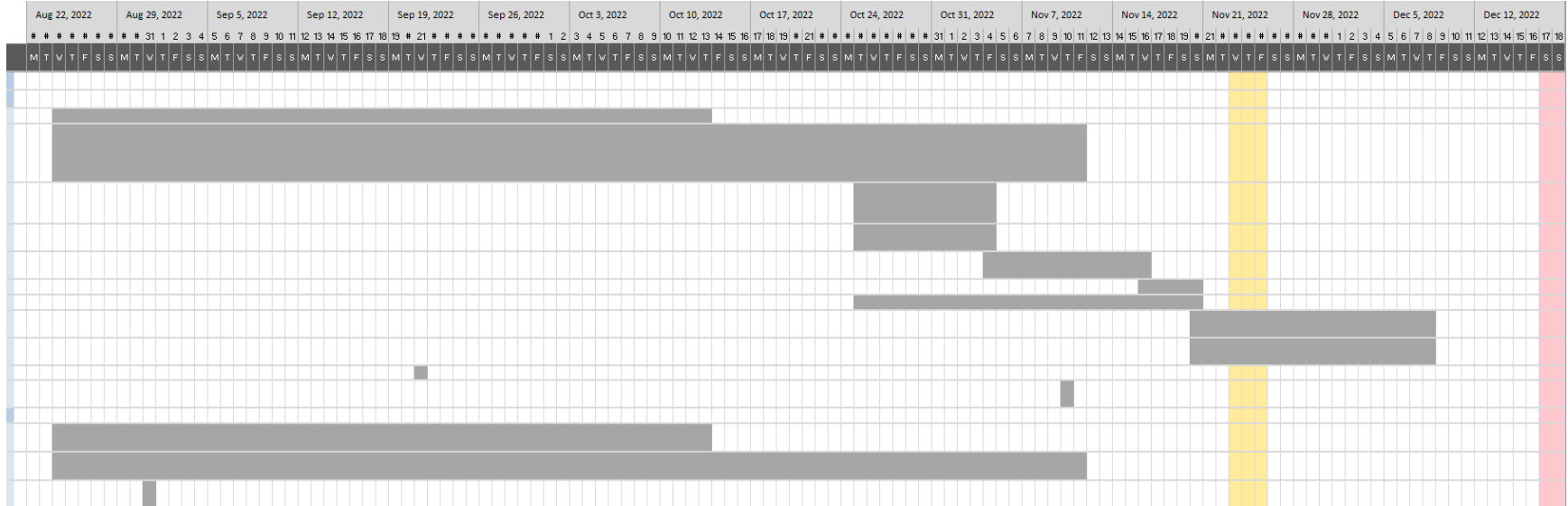


Figure 52: Image of the Gantt Chart used for Goal 1. Rows in the bottom of the picture correspond to the tasks in the top picture.



TASK	ASSIGNED TO	PROGRESS	START	END
<b>Goal 2</b>				
Objective				
2. Order/Receive laser scanner	Maria	100%	10/27/22	11/4/22
3. Practice/train in use of laser scanner on objects at WPI	Whole Team	100%	11/7/22	11/10/22
<b>Goal 4</b>				
1. Complete Software Training	Whole Team	100%	8/24/22	10/13/22

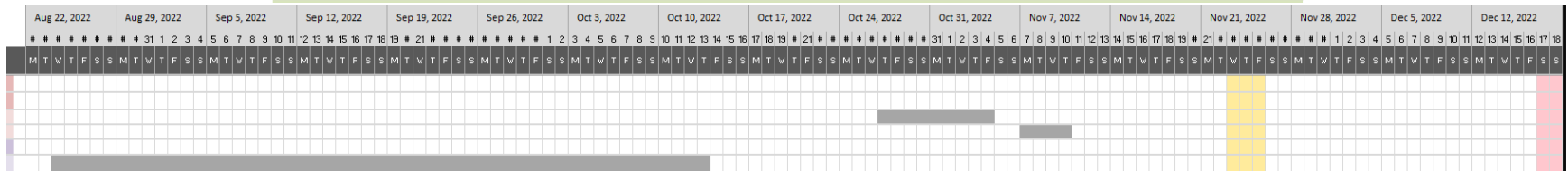


Figure 53: Image of the Gantt Chart used for Goals 2 and 3. Rows in the bottom of the picture correspond to the tasks in the top picture.

TASK	ASSIGNED TO	PROGRESS	START	END
<b>Writing Goals</b>				
1. Write Report Sections describing history of each aircraft	Whole Team	100%	8/24/22	10/13/22
2. Write report sections describing performance capabilities of each aircraft	Maria, Aaron, Gabi, Nick P	100%	8/24/22	11/15/22
3. Write report sections describing methodology for creation of solid (CAD) model from 2D plan	Maria, Nick O	100%	10/25/22	11/6/22
4. Write report sections describing Fluent simulation, including governing equations and description of boundary conditions.	Maria, Nick O, Amaya	100%	11/18/22	11/28/22
5. Write report section presenting cases investigated and results for CBY-3	Maria, Nick O	100%	12/8/22	12/18/22
6. Write report section presenting cases investigated and results for DC-3	Maria, Nick O	100%	12/8/22	12/18/22
7. Write report section comparing CBY-3 to DC-3 with respect to flight characteristics, e.g. lift/drag characteristics; did the lifting body fuselage design really help?--if so, how much?	Maria, Nick O	100%	12/8/22	12/18/22
8. Write report section comparing CBY-3 to DC-3 with respect to CBY-3 box shaped fuselage vs. the DC-3 tubular design	Maria, Nick O	100%	12/8/22	12/18/22
9. Write report section comparing CBY-3 to DC-3 with respect to CBY-3 engine location arrangement vs. that of the DC-3	Maria, Nick O	100%	12/8/22	12/18/22
<b>Peer Review</b>				
Introduction, Background (1,2)		100%	10/10/22	10/16/22
Methodology (3)		100%	11/6/22	11/10/22
Methodology (4)		100%	11/28/22	12/2/22
Fluent Report (5,6,7,8,9)		100%	12/16/22	12/19/22

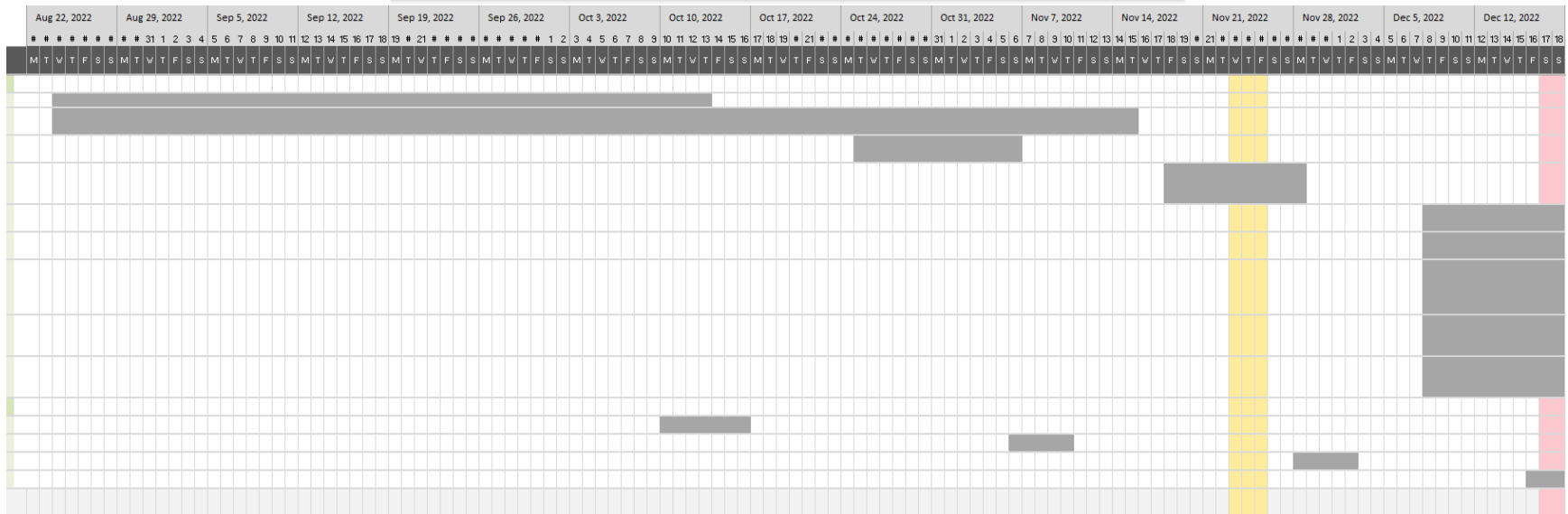


Figure 54: Image of the Gantt Chart used for Writing Goals. Rows in the bottom of the picture correspond to the tasks in the top picture.